UCLouvain

FACULTE DES SCIENCES

Faculté des sciences

The Chen-Yang volume conjecture for knots in handlebodies

Auteur : James Gosselet

Promoteurs : Fathi Ben Aribi, Pedro Vaz

Lecteurs : Pascal Lambrechts, Marino Gran

Année académique 2020-2021

UNIVERSITÉ CATHOLIQUE DE LOUVAIN
FACULTÉ DES SCIENCES
ÉCOLE DE MATHÉMATIQUES

The Chen-Yang volume conjecture for knots in handlebodies

James Gosselet
Advisors: Fathi Ben Aribi, Pedro Vaz
Readers: Pascal Lambrechts, Marino Gran

Master thesis
June 2021

Contents

Chapter 1

Introduction

Quantum topology began in 1984 with the definition of the Jones Polynomial [7]. Since then, several new invariants of knots and 3-manifolds were defined and, inspired by quantum field theories in physics, the *volume conjecture* of Kashaev [8] and its variants rose to be one of the the most studied conjectures in quantum topology. What is intriguing about these volume conjectures is that they link quantum invariants of manifolds to the hyperbolic structure of these manifolds. In [3], Chen-Yang propose a volume conjecture using a family $\{TV_{r,2}\}_{r\in\mathbb{N}_{\geq 3}}$ of Turaev-Viro type invariants for compact 3-manifolds.

Conjecture 1.1 (Conjecture 1.1, [3], Chen-Yang)**.** *Let M be a compact hyperbolic 3-manifold. Then for r running over all odd integers such that $r \geq 3$,*

$$\lim_{r\to\infty} \frac{2\pi}{r-2} \log\left(TV_{r,2}(M)\right) = Vol_H(M),$$

where $Vol_H(M)$ is the hyperbolic volume of M.

This conjecture has since then been proved [4, 11, 14] or numerically tested [3] for several hyperbolic 3-manifolds, mostly for manifolds without boundary, but also manifolds with toroidal boundary and manifolds with totally geodesic boundary of genus $g \geq 2$. However, there is currently no test of this conjecture for a hyperbolic 3-manifold with a boundary which has both a toroidal component and a totally geodesic boundary component of genus $g \geq 2$. In this thesis, we thus propose to test the Chen-Yang hyperbolic volume conjecture for a family of 3-manifolds $\{M_g\}_{g\in\mathbb{N}_{\geq 2}}$, that can be seen as knot exteriors in a g-handlebody. Recall that a g-handlebody is the boundary-connected sum of a collection of g solid tori.

We will start in Chapter 2 by defining what the triangulation of a topological space is and what an ideal triangulation is. Section 2.1 introduces a lot of notations that are used throughout the thesis and should be carefully understood before reading the rest of the paper. The rest of chapter is focused on describing the ideal triangulations $\mathcal{T}_g$ of

the 3-manifolds M_g, defined by Frigerio in [5, Section 1]. In the process, we will prove the following proposition.

Proposition 1.2 (Proposition 2.19)**.** *The 3-manifold M_g admits an ordered ideal triangulation $\mathcal{T}_g$.*

Lastly, we will define what the comb representation of an ordered triangulation is and illustrate it with the comb representation of $\mathcal{T}_2$. This is useful as a more compact way of writing the triangulation, but will not be used in the rest of the thesis.

Chapter 3 explains some notions of hyperbolic geometry with the only goal of computing the hyperbolic volumes $Vol_H(M_g)$. This is not the main topic of this thesis and this section can be glossed over by a reader in a hurry.

In Chapter 4, we will define the Turaev-Viro invariants $TV_{r,s}(M, \mathcal{T})$. In order to achieve that, we need first to define admissible colourings c of a triangulation. We will derive from $\mathcal{T}_g$ the set of all its admissible colourings $\mathcal{A}_r(M_g, \mathcal{T}_g)$. We will then prove the following proposition.

Proposition 1.3 (Proposition 4.8)**.** *An admissible colouring of $\mathcal{T}_g$ has to satisfy a certain set of admissibility conditions which are equivalent to another set of conditions.*

The proof of Proposition 1.3 is quite lengthy, technical but can give insights on how to simplify admissibility conditions. The new set of conditions given by Proposition 1.3 will be used later on in Chapter 6. We will lastly define the Turaev-Viro invariants $TV_{r,s}(M, \mathcal{T})$ as a sum over all admissible colourings $\mathcal{A}(M, \mathcal{T})$ and we will apply this definition to $(M_2, \mathcal{T}_2)$ and $(M_3, \mathcal{T}_3)$.

Chapter 5 is the central part of this thesis. For $(M_2, \mathcal{T}_2)$ and $(M_3, \mathcal{T}_3)$, we give a reminder of their respective hyperbolic volume $Vol_H(M)$, triangulation $\mathcal{T}$ and Turaev-Viro invariants $TV_{r,2}(M, \mathcal{T})$. We define $QV_{r,2}(M) := \frac{2\pi}{r-2} \log(TV_{r,2}(M, \mathcal{T})$, plot the values computed in Section 6.3 and look at the behaviour of $QV_{r,2}(M_2)$ and $QV_{r,2}(M_3)$ for increasing values of r.

Numerical test 1.4 (Numerical tests 5.2, 5.3 and 5.4)**.** *The graph of $QV_{r,2}(M_2)$ shows a converging behaviour up to $r = 33$ and an unexpected and unusual increase after $r = 33$. The graph of $QV_{r,2}(M_3)$ shows a converging behaviour up to $r = 31$.*

Chapter 6 goes into the details of our code. We start in Section 6.1 by computing the hyperbolic volumes of M_g and the common hyperbolic volume of the tetrahedra of $\mathcal{T}_g$

using the theorems and propositions of Chapter 3. We get the values listed in Figure 1.1. Then, we construct several functions in Section 6.2 following definitions of Section 4.2 with the goal to compute $TV_{r,s}(M_2, \mathcal{T}_2)$ and $TV_{r,s}(M_2, \mathcal{T}_2)$. We conclude in Section 6.3, by computing $QV_{r,2}(M_2)$ and $QV_{r,2}(M_3)$ for increasing values of r.

g	$Vol_H(T_g)$	$Vol_H(M_g)$
2	2.007682006682397	12.046092040094381
3	2.2547631818606026	18.03810545488482
4	2.3603494908554774	23.603494908554772
5	2.415787949187158	28.989455390245897
6	2.448617485457304	34.28064479640226
7	2.469695490891516	39.51512785426426
8	2.484045062029212	44.71281111652581
9	2.494259571737797	49.88519143475594
10	2.5017908556003303	55.039398823207264
100	2.5369350366401	512.4608774013002
1000	2.5373497508910896	5079.774201283962

Figure 1.1: The hyperbolic volumes of M_g and one tetrahedron T_g of $\mathcal{T}_g$ for various values of g.

My contributions The propositions and numerical tests stated in this introduction are original results. If not stated, all figures and listings in this paper are the result of my own work. This includes notably the coloured triangulations and the code of Chapter 6. If inspiration has been taken from other works, it is explicitly referenced.

Prerequisites This thesis is intended to be readable by any Master student with basic notions in the following topics:

- Topology (homeomorphisms, manifolds, boundaries, components, handlebodies, quotient spaces, neighbourhoods, ...),
- Geometry (geodesics, embeddings, metric space, isometries, dihedral angles, ...),
- Knot theory (knot exterior, ...),
- Programming (Python, loops, functions, ...).

Acknowledgements I would like to thank my two promoters, Fathi Ben Aribi and Pedro Vaz for their intellectual and emotional support throughout this Master's thesis. Fathi Ben Aribi greatly helped me to understand the mathematical foundations of the volume conjecture and gave me a lot of good commentaries on the intermediary versions that helped me improve the quality of this document. They both gave me strong advice on how to work and guided me trough the research and writing process. They were also very understanding of the difficulties that came with it. I would also like to thank all my mathematics professors throughout the years that brought me the passion of mathematics with which I wrote this thesis.

Chapter 2

Triangulations

For $g \in \mathbb{N}_{\geq 2}$, let $\Sigma_g := \#_{i=1}^{g} (S^1 \times S^1)$ be the connected sum of g tori, i.e a surface of genus g.

2.1 Definitions

2.1.1 Tetrahedra

Definition 2.1. The *standard tetrahedron* (see Figure 2.1) is defined as

$$T_{st} := \left\{ (x, y, z) \in \mathbb{R}^3 \;\middle|\; \begin{array}{l} 0 \leq x, \\ 0 \leq y, \\ 0 \leq z, \\ 0 \leq x + y + z \leq 1 \end{array} \right\}.$$

The *vertices* of T_{st} are denoted by $s_0 := (0, 0, 0)$, $s_1 := (1, 0, 0)$, $s_2 := (0, 1, 0)$ and $s_3 := (0, 0, 1)$.

The *edges* of T_{st} are denoted by $a_{ij} := \left\{ t \cdot s_i + (1 - t) \cdot s_j \in \mathbb{R}^3 \,\middle|\, 0 \leq t \leq 1 \right\}$ for $i, j \in \{0, 1, 2, 3\}$ such that $i < j$.

The *faces* of T_{st} are denoted by

$$c^i = c_{jkl} = \left\{ t_1 \cdot s_j + t_2 \cdot s_k + (1 - t_1 - t_2) \cdot s_l \in \mathbb{R}^3 \;\middle|\; \begin{array}{l} 0 \leq t_1, \\ 0 \leq t_2, \\ t_1 + t_2 \leq 1 \end{array} \right\}$$

for $i, j, k, l \in \{0, 1, 2, 3\}$ such that $j < k < l$ and $i \notin \{j, k, l\}$.

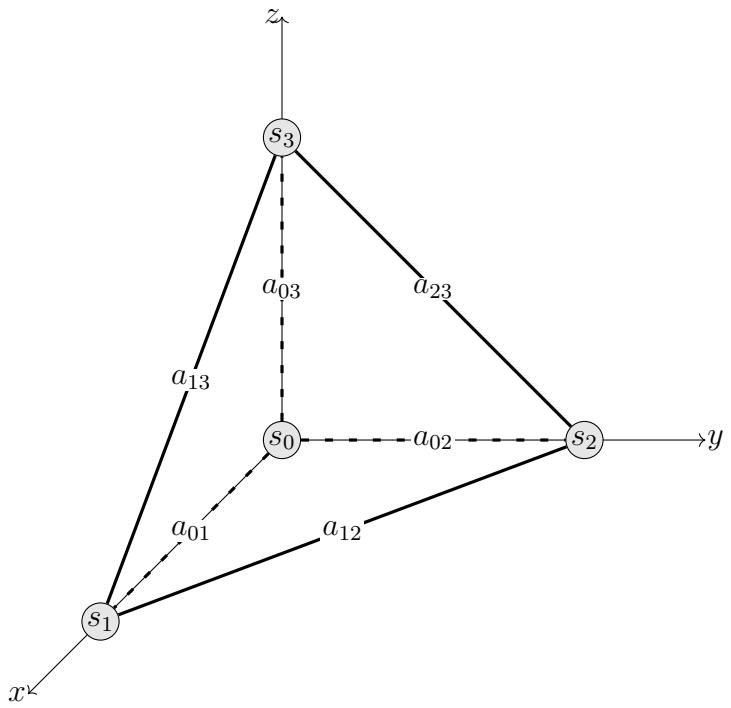

Figure 2.1: The standard tetrahedron T_{st} with its vertices $s_0 = (0,0,0)$, $s_1 = (1,0,0)$, $s_2 = (0,1,0)$, $s_3 = (0,0,1)$ and edges a_{01}, a_{02}, a_{03}, a_{12}, a_{13}, a_{23}.

Definition 2.2. A *tetrahedron* (T, h) is the pair of a topological 3-manifold with boundary T (see Figure 2.2) and an homeomorphism $h : T_{st} \to T$. We will sometimes refer to (T, h) simply as T.

The *vertices* of T are the $v_i := h(s_i)$ for $i \in \{0, 1, 2, 3\}$.

The *edges* of T are the $e_{ij} := h(a_{ij})$ for $i, j \in \{0, 1, 2, 3\}$ such that $i < j$.

The *faces* of T are the $f^i := h(c^i)$ for $i \in \{0, 1, 2, 3\}$.

Remark 2.3. The homeomorphism h might not be orientation-preserving.

Definition 2.4. Let $X = \{(T_1, h_1), (T_2, h_2), ..., (T_n, h_n)\}$ be a finite collection of distinct tetrahedra. We define:

- its *0-skeleton* as $X^0 := \left\{ h_l(s_i) \;\middle|\; \begin{array}{l} i \in \{0,1,2,3\}, \\ l \in \{1,2,...,n\} \end{array} \right\}$,
- its *1-skeleton* as $X^1 := \left\{ h_l(a_{ij}) \;\middle|\; \begin{array}{l} i,j \in \{0,1,2,3\} \text{ such that } i<j, \\ l \in \{1,2,...,n\} \end{array} \right\}$,

- its *2-skeleton* as $X^2 := \left\{ h_l(c^i) \,\middle|\, \begin{array}{l} i \in \{0,1,2,3\}, \\ l \in \{1,2,...,n\} \end{array} \right\}$,
- its *3-skeleton* as $X^3 := \{T_1, T_2, ..., T_n\}$.

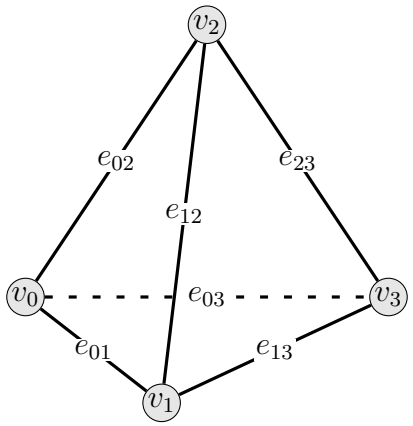

Figure 2.2: A topological 3-manifold with boundary T, homeomorphic to T_{st}, with its vertices v_0, v_1, v_2, v_3 and edges e_{01}, e_{02}, e_{03}, e_{12}, e_{13}, e_{23}.

2.1.2 Triangulations of topological spaces

Definition 2.5. Let $l, p \in \{0,1,2,3\}$. Let f^l and f^p be two faces of T_{st} and $\tilde{\psi} : f \to f'$ be an affine homeomorphism. We say that $\tilde{\psi}$ *preserves the order of the vertices* if for $i, j, k, m, n, o \in \{0,1,2,3\}$ such that $i < j < k$, $i, j, k \neq l$, $m < n < o$ and $m, n, o \neq p$, we have $\tilde{\psi}(s_i) = s_m$, $\tilde{\psi}(s_j) = s_n$ and $\tilde{\psi}(s_k) = s_o$. In other words, the vertex with the smallest (resp. middle, biggest) index is sent to the vertex with the smallest (resp. middle, biggest) index.

Definition 2.6. Let (T, h) and (T', h') be two tetrahedra. For two distinct faces $f \subset T$ and $f' \subset T'$, we call an *identification map* of these two faces a function $\psi_{ff'} : f \to f'$ such that $\psi_{ff'}$ is an homeomorphism and $\tilde{\psi}_{ff'} = (h')^{-1} \circ \psi_{ff'} \circ h : h^{-1}(f) \to (h')^{-1}(f')$ is affine. If $\tilde{\psi}_{ff'}$ preserves the order of the vertices, then we call $\psi_{ff'}$ an *ordered identification map* (see Figure 2.3 for an illustrated example).

Remark 2.7. In Definition 2.6, since h, h' and $\psi_{ff'}$ are homeomorphisms, $\tilde{\psi}_{ff'}$ is well-defined and an homeomorphism.

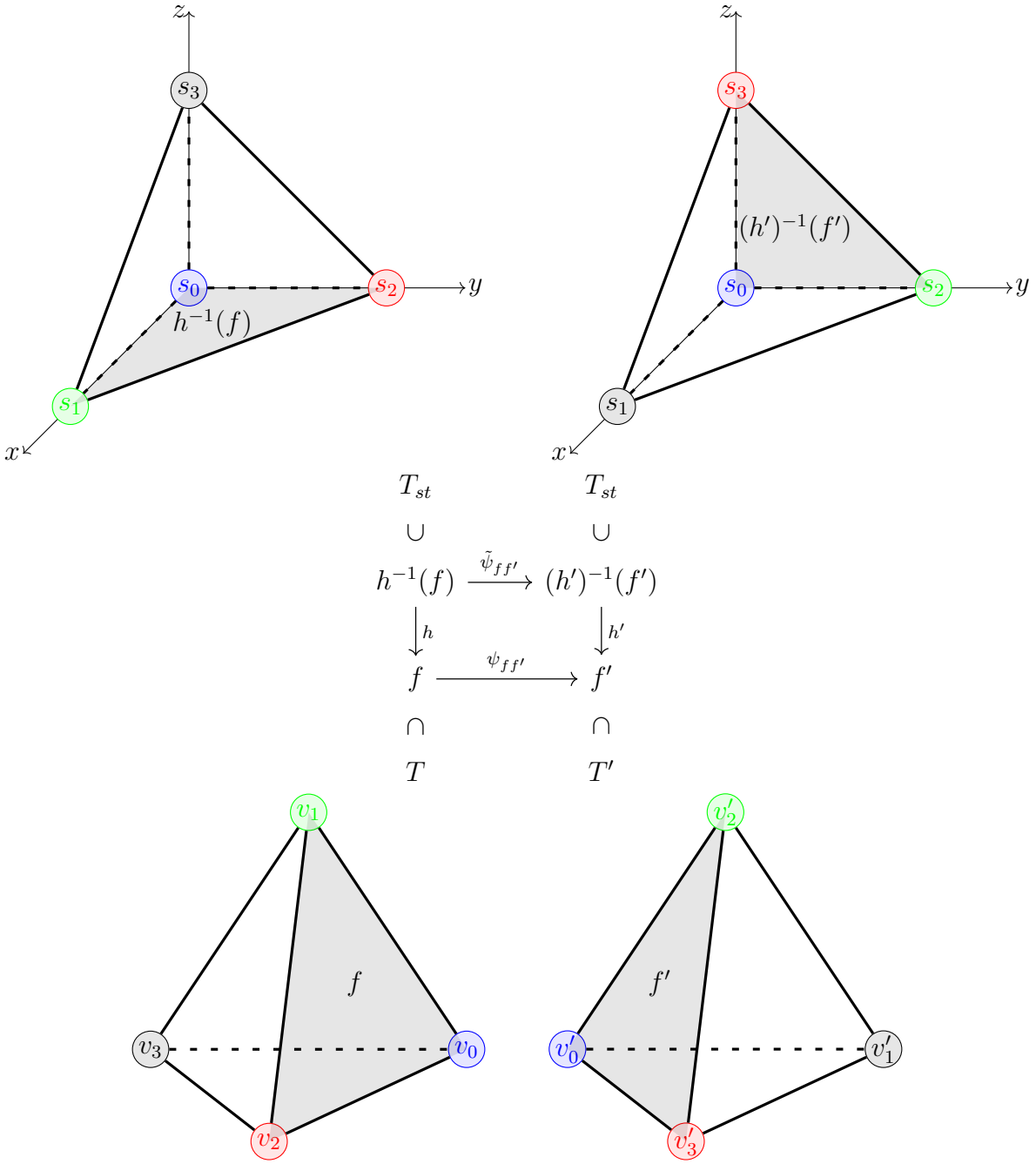

Figure 2.3: An example of an ordered identification map of two faces f and f': each point of color is sent to the points of same color via the homeomorphisms.

Definition 2.8. Let N be a topological space. Let $X = \{(T_1, h_1), (T_2, h_2), ..., (T_n, h_n)\}$ be a finite collection of distinct tetrahedra. Let $\Psi = \{\psi_1, ..., \psi_{2n}\}$ be a finite collection of identification maps of two faces of these tetrahedra such that for any face $f \in X^2$ there exist a unique distinct face $f' \in X^2$ and a unique $\psi \in \Psi$ such that $\psi = \psi_{ff'}$ or $\psi^{-1} = \psi_{ff'}$.

We say that N admits a *triangulation* (X, Ψ) if $\left(\coprod_{i=0}^{n} T_i\right)/\sim$ is homeomorphic to N where the equivalence relation $\sim$ on $\coprod_{i=0}^{n} T_i$ is defined by: $x \sim y$ if and only if $(x = y)$ or $(\exists \psi \in \Psi$ such that $y \in \{\psi(x), \psi^{-1}(x)\})$.

We say that (X, Ψ) is *ordered* if for all $\psi \in \Psi$, ψ is an ordered identification map, i.e preserves the order of the vertices.

Remark 2.9. Everywhere except possibly at some vertices, N is a manifold.

Definition 2.10. Let N be a topological space which admits a triangulation (X, Ψ). We define:

- the *0-skeleton* as $X^0_\sim = X_0/\sim$ and denote its members by the letter ν,
- its *1-skeleton* as $X^1_\sim = X_1/\sim$ and denote its members by the letter η,
- its *2-skeleton* as $X^2_\sim = X_2/\sim$ and denote its members by the letter ϕ,
- its *3-skeleton* as $X^3_\sim = X_3/\sim$ and denote its members by the letter Δ.

Remark 2.11. You can give to each edge $e \in X^1$ an orientation from the vertex with lowest index to the vertex with biggest index such that on each tetrahedron, for all $i \in \{0, 1, 2, 3\}$, exactly i edges points to the vertex v_i. If a triangulation is ordered, for each $\eta \in X^1_\sim$, all the edges $e \in \eta$ have the same orientation. Hence, there is an induced orientation on each edge $\eta \in X^1_\sim$ of the triangulation.

2.1.3 Ideal triangulations of 3-manifolds

Recall that for $g \in \mathbb{N}_{\geq 2}$, $\Sigma_g := \#_{i=1}^{g} (S^1 \times S^1)$ is the connected sum of g tori, i.e a surface of genus g.

Definition 2.12. Let N be a topological space which admits a triangulation (X, Ψ). Let $\nu \in X^0_\sim$. Let U_ν denote its open neighbourhood in N. We say that:

- ν is *regular* if ∂U_ν is homeomorphic to S^2,
- ν is *ideal* if ∂U_ν is homeomorphic to $S^1 \times S^1$,
- ν is *hyperideal* if ∂U_ν is homeomorphic to Σ_g for some $g \in \mathbb{N}_{\geq 2}$.

Definition 2.13. Let M be a compact 3-manifold with boundary $\partial M = \partial M_1 \cup \partial M_2 \cup ... \cup \partial M_{p+q}$ which has for $k \in \{1, ..., p\}$, ∂M_k homeomorphic to $S^1 \times S^1$ and for $k \in \{p+1, ..., p+q\}$, ∂M_k homeomorphic to Σ_{g_k} for some $g_k \in \mathbb{N}_{\geq 2}$. Let N be a topological space which admits a triangulation (X, Ψ). Let $I = \{\nu \in X^0_\sim \,|\, \nu \text{ is ideal}\} = \{\nu^i_1, \nu^i_2, ..., \nu^i_p\}$ and $H = \{\nu \in X^0_\sim \,|\, \nu \text{ is hyperideal}\} = \{\nu^h_1, \nu^h_2, ...\nu^h_q\}$. Let U_ν denote a small open neighbourhood in N of $\nu \in X^0_\sim$.

We say that M admits the *ideal triangulation* $\mathcal{T} = (X, \Psi, I, H)$ if M is homeomorphic to $N \setminus \{U_{\nu^i_1}, ..., U_{\nu^i_p}, U_{\nu^h_1}, ..., U_{\nu^h_q}\}$.

We say that $\mathcal{T}$ is *ordered* if for all $\psi \in \Psi$, ψ is an ordered identification map, i.e preserves the order of the vertices.

Remark 2.14. If N admits a triangulation, we have that everywhere except at the ideal and hyperideal vertices, N is a 3-manifold, thus removing a small open neighbourhood of each of those vertices ensures that we obtain a compact 3-manifold with boundary.

2.2 A family of manifolds M_g

This section follows closely the construction in [5, Section 1]. Let $g \in \mathbb{N}_{\geq 2}$. Let S^3 be the one point compactification of $\mathbb{R}^3$.

Definition 2.15. Let $\Gamma_g \subset S^3$ be the graph shown on the left in Figure 2.4. Let us denote by Γ_g^0 and Γ_g^1 the two connected components of Γ_g, where Γ_g^0 is a knot and Γ_g^1 has two vertices and $g+1$ edges. Let $U(\Gamma_g^0)$ be an open regular neighbourhood of Γ_g^0. Let $U(\Gamma_g^1)$ be an open regular neighbourhood of Γ_g^1.

We define M_g as the compact 3-manifold $S^3 \setminus \{U(\Gamma_g^0), U(\Gamma_g^1)\}$ with boundary $\partial M = \partial M^1 \cup \partial M^2$ such that $\partial M_1 = \partial U(\Gamma_g^0) \cong S^1 \times S^1$ and $\partial M^2 = \partial U(\Gamma_g^1) \cong \Sigma_g$.

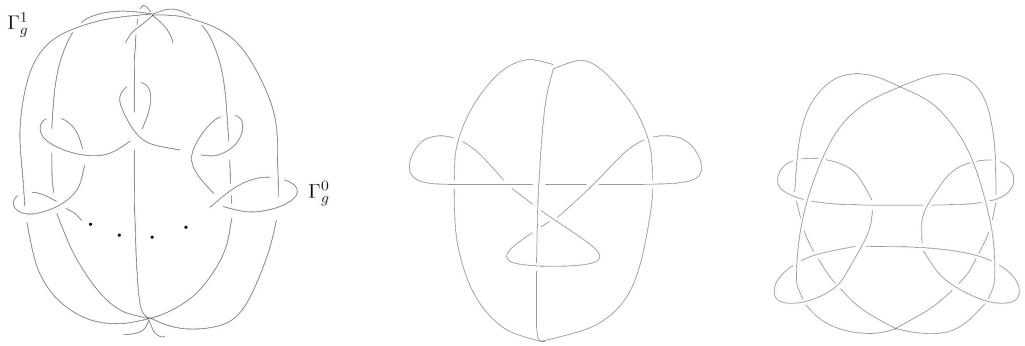

Figure 2.4: Γ_g has two components: Γ_g^0 is a knot and Γ_g^1 is a graph with $g+1$ edges and two vertices. From left to right: Γ_g, Γ_2 and Γ_3, Source: [5, Figure 1]

Remark 2.16. The 3-manifold M_g is the exterior of a knot in the handlebody of genus g as seen in Figure 2.5 for the case $g = 2$.

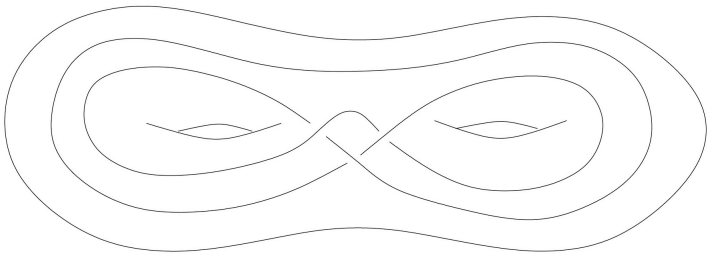

Figure 2.5: The 3-manifold M_2 as a knot complement in the handlebody of genus 2. Source: [5, Figure 3]

2.2.1 An ideal triangulation of M_g

In [5, Section 2], Frigerio constructs an ideal triangulation of M_g. This construction is illustrated for the cases $g = 2$ and $g = 3$ in Figure 2.6.

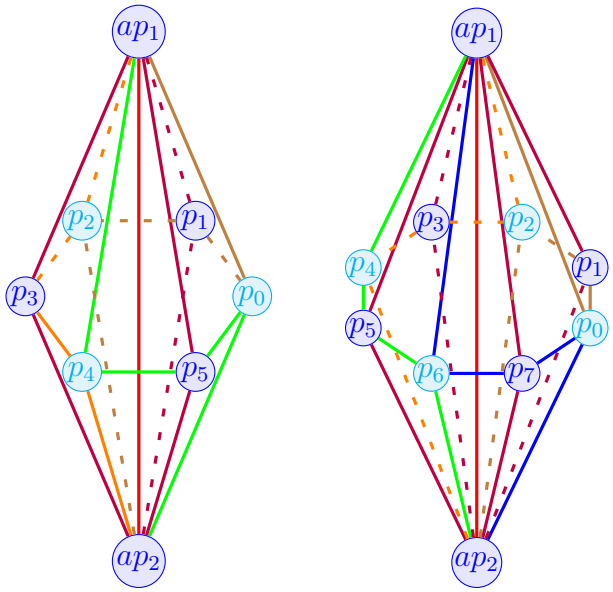

Figure 2.6: Representation of Y_2 (left) and Y_3 (right) with the red vertical edge between the two apices and identified edges and vertices have the same color.

Let P_g be the double cone with apices ap_1 and ap_2 and based on the regular $(2g+2)$-gon whose vertices are p_0, p_1, ..., p_{2g+1}. Let $\mathring{P}_g$ be P_g with its vertices removed. Let Y_g be the topological space obtained by gluing the faces of $\mathring{P}_g$ according to the following rules:

- For any $i = 0, 2, ..., 2g-2$, the face $[ap_1, p_i, p_{i+1}]$ is identified with the face $[p_{i+1}, p_{i+2}, v_2]$ (with v_1 identified with p_{i+1}, p_i identified with p_{i+2} and p_{i+1} identified with ap_2),
- The face $[ap_1, p_{2g}, p_{2g+1}]$ is identified with the face $[p_{2g+1}, p_0, v_2]$ (with v_1 identified with p_{2g+1}, p_{2g} identified with p_0 and p_{2g+1} identified with ap_2),
- For any $i = 1, 3, ..., 2g-1$, the face $[ap_1, p_i, p_{i+1}]$ is identified with the face $[p_{i+2}, v_2, p_{i+1}]$ (with ap_1 identified with p_{i+2}, p_i identified with ap_2 and p_{i+1} identified with p_{i+1}).
- The face $[ap_1, p_{2g+1}, p_0]$ is identified with the face $[p_1, v_2, p_0]$ (with ap_1 identified with p_1, p_{2g+1} identified with ap_2 and p_1 identified with p_1).

Proposition 2.17 (Proposition 2.1, [5]). *For any $g \geq 2$, Y_g is homeomorphic to the interior of M_g.*

We can subdivide P_g into $2g+2$ tetrahedra by adding the vertical edge between the two apices ap_1 and ap_2 (in red in Figure 2.6). Such tetrahedra give an ideal triangulation of M_g that we define more rigorously in next section.

2.2.2 The ordered ideal triangulation $\mathcal{T}_g$ of M_g

Let $X_g = \{(T_1, h_1), (T_2, h_2), ..., (T_{2g+2}, h_{2g+2})\}$ be a collection of $2g+2$ distinct tetrahedra. For $i \in \{1, 2, 3, ..., 2g+2\}$ and $j \in \{0, 1, 2, 3\}$, let v_j^i denote the vertex v_j of T_i. For $i \in \{1, 2, 3, ..., 2g+2\}$ and $j, k, l \in \{0, 1, 2, 3\}$ such that $j < k < l$, let f_{jkl}^i denote the face f_{jkl} of T_i. Let $\Psi_g = \{\psi_1, ..., \psi_{4g+4}\}$ where its elements are identification maps as follows :

- For $i \in \{1, ..., g+1\}$, $\psi_i : f_{012}^{2i-1} \subset T_{2i-1} \to f_{012}^{2i} \subset T_{2i}$ such that $\psi_i(v_0^{2i-1}) = v_0^{2i}$, $\psi_i(v_1^{2i-1}) = v_1^{2i}$ and $\psi_i(v_2^{2i-1}) = v_2^{2i}$,
- $\psi_{g+2} : f_{023}^{2g+2} \subset T_{2g+2} \to f_{023}^1 \subset T_1$ such that $\psi_{g+2}(v_0^{2g+2}) = v_0^1$, $\psi_{g+2}(v_2^{2g+2}) = v_2^1$ and $\psi_{g+2}(v_3^{2g+2}) = v_3^1$,
- For $i \in \{1, ..., g\}$, $\psi_{g+2+i} : f_{023}^{2i} \subset T_{2i} \to f_{023}^{2i+1} \subset T_{2i+1}$ such that $\psi_{g+2+i}(v_0^{2i}) = v_0^{2i+1}$, $\psi_{g+2+i}(v_2^{2i}) = v_2^{2i+1}$ and $\psi_{g+2+i}(v_3^{2i}) = v_3^{2i+1}$,
- For $i \in \{1, ..., g+1\}$, $\psi_{2g+2+i} : f_{123}^{2i-1} \subset T_{2i-1} \to f_{013}^{2i} \subset T_{2i}$ such that $\psi_{2g+2+i}(v_1^{2i-1}) = v_0^{2i}$, $\psi_{2g+2+i}(v_2^{2i-1}) = v_1^{2i}$ and $\psi_{2g+2+i}(v_3^{2i-1}) = v_3^{2i}$,
- $\psi_{3g+4} : f_{013}^{2g+2} \subset T_{2g+2} \to f_{123}^1 \subset T_1$ such that $\psi_{3g+4}(v_0^{2g+2}) = v_1^1$, $\psi_{3g+4}(v_1^{2g+2}) = v_2^1$ and $\psi_{3g+4}(v_3^{2g+2}) = v_3^1$,
- For $i \in \{1, ..., g\}$, $\psi_{3g+4+i} : f_{013}^{2i} \subset T_{2i} \to f_{123}^{2i+1} \subset T_{2i+1}$ such that $\psi_{3g+4+i}(v_0^{2i}) = v_1^{2i+1}$, $\psi_{3g+4+i}(v_1^{2i}) = v_2^{2i+1}$ and $\psi_{3g+4+i}(v_3^{2i}) = v_3^{2i+1}$.

Remark 2.18. The $g+2$ first identification maps corresponds to the gluing of the tetrahedra along the red vertical edge as in Figure 2.6. The other identification maps corresponds to the identifications in Section 2.2.1.

The triangulation (X_g, Ψ_g) has:

- a 0-skeleton $X^0_\sim = \{\nu_1, \nu_2\}$,
- a 1-skeleton $X^1_\sim = \{\eta_1, \eta_2, ..., \eta_{g+3}\}$,
- a 2-skeleton $X^2_\sim = \{\phi_1, \phi_2, ..., \phi_{4g+4}\}$,
- a 3-skeleton $X^3_\sim = \{\Delta_1, \Delta_2, ..., \Delta_{2g+2}\}$.

Proposition 2.19. *The triangulation (X_g, Ψ_g) is ordered.*

Proof. For $i \in \{1, 2, ..., 2g+2\}$, the tetrahedron $(T_i, h_i) \in X_g$ corresponds to the tetrahedron with vertices p_{i-1}, p_i, ap_1 and ap_2 as defined in Subsection 2.2.1. However, there was some freedom when choosing the homeomorphisms h_i. More specifically, we could chose which standard vertex s_i was sent to which vertex of T_i. For $i \in \{1, 3, 5, ..., 2g+1\}$, we chose that $h_i(s_0) = v^i_0 = ap_2$, $h_i(s_1) = v^i_1 = p_i$, $h_i(s_2) = v^i_2 = ap_1$ and $h_i(s_3) = v^i_3 = p_{i-1}$. For $i \in \{2, 4, 6, ..., 2g+2\}$, we chose that $h_i(s_0) = v^i_0 = ap_2$, $h_i(s_1) = v^i_1 = p_{i-1}$, $h_i(s_2) = v^i_2 = ap_1$ and $h_i(s_3) = v^i_3 = p_i$. This choice gives for the triangulation the identification maps in Ψ_g previously defined and we see that each of these identification maps preserves the order of the vertices. By Definition 2.13, this means that (X_g, Ψ_g) is ordered. □

Proposition 2.20. *The 3-manifold M_g admits an ordered ideal triangulation $\mathcal{T}_g = (X_g, \Psi_g, I_g, H_g)$ (see Figures 2.7 and 2.8 for the cases $g = 2$ and $g = 3$).*

Proof. Let $N_g = \left(\coprod_{i=0}^{n} T_i\right) / \sim$. Let U_ν denote the open neighbourhood in N of $\nu \in X^0_\sim$. By Proposition 2.17, $N_g - X^0_\sim$ is homeomorphic to the interior of M_g. Thus, M_g is homeomorphic to $N - \{U_{\nu_1}, U_{\nu_2}\}$. Since ∂U_{ν_1} is homeomorphic to $S_1 \times S_1$ and ∂U_{ν_2} is homeomorphic to Σ_g, we set $I_g = \{\nu_1\}$ and $H_g = \{\nu_2\}$ (see Remark 2.21). By Definition 2.13, this means that M_g admits an ideal triangulation $\mathcal{T}_g = (X_g, \Psi_g, I_g, H_g)$. By Proposition 2.19, this triangulation is ordered. □

Remark 2.21. In [5, Section 2], by looking at the induced triangulation on the neighbourhood of the vertices, Frigerio points out that the equivalence class $\nu_1 = \{p_0, p_2, p_4, ..., p_{2g}\}$ (which is $\{v^1_3, v^2_3, ..., v^{2g+2}_3\}$ with our notations) is ideal, i.e that U_{ν_1} is homeomorphic to $S_1 \times S_1$, while the equivalence class ν_2 is hyperideal, i.e that U_{ν_2} is homeomorphic to Σ_g.

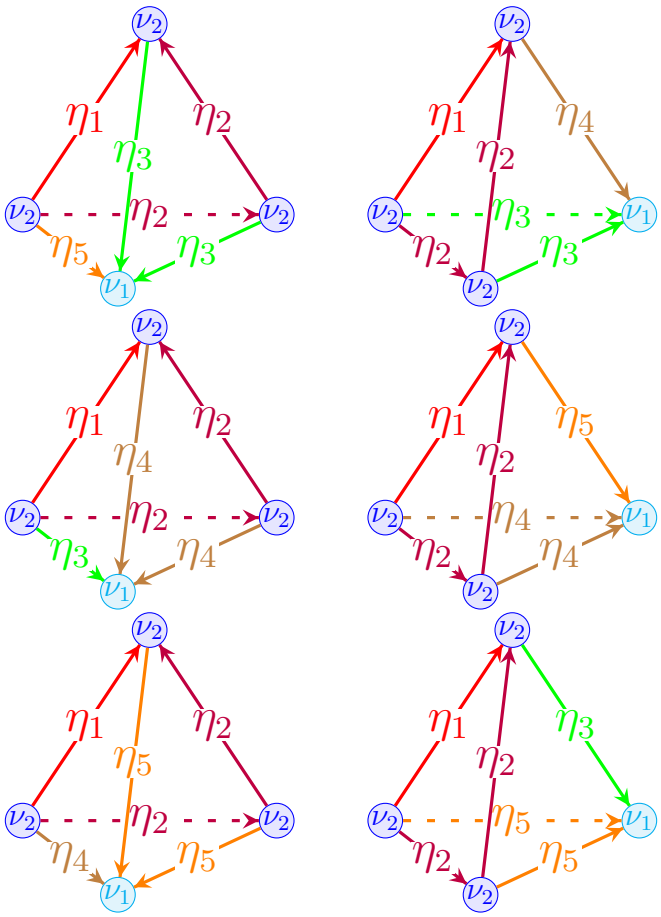

Figure 2.7: Representation of the ordered ideal triangulation $\mathcal{T}_2$ of the 3-manifold M_2

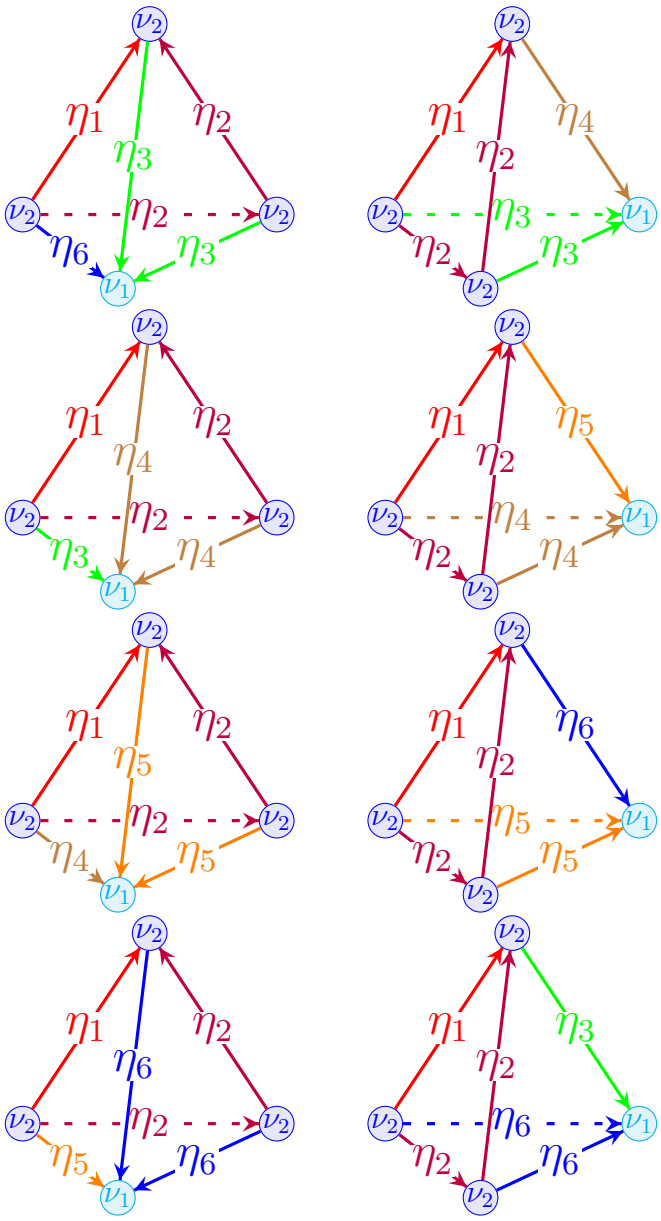

Figure 2.8: Representation of the ordered ideal triangulation $\mathcal{T}_3$ of the 3-manifold M_3

2.3 Comb representations

The comb representation of a triangulation has been introduced in [9, Example 4.1] and we borrowed the following definition from [1, Section 2.1].

Definition 2.22. A comb C is a line together with four orthogonal spikes pointing in the same direction. The spikes are numbered 0, 1, 2 and 3 going from left to right, with the spikes pointing upward (see Figure 2.9).

To a tetrahedron (T, h), we can associate a comb $C(T, h)$ as in figure 2.9, each spike numbered i corresponding to the face f^i that is opposed to the vertex v_i for $i \in \{0, 1, 2, 3\}$.

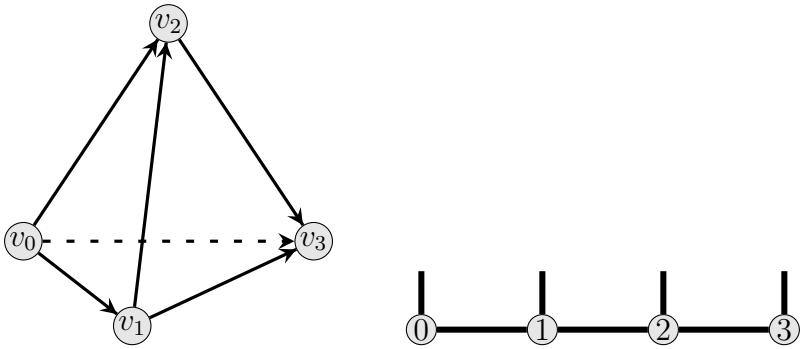

Figure 2.9: An ordered tetrahedron (T, h) and its associated comb $C(T, h)$.

Definition 2.23. Let N be a topological space which admits an ordered triangulation (X, Ψ). For $i \in \{0, 1, 2, 3\}$, we define $x_i : X^3_\sim \to X^2_\sim$ the map such that $x_i(\Delta) = \phi$ where $\Delta = [T]$ is the equivalence class of T and $\phi = [f^i]$ is the equivalence class of the face opposed to the vertex $v_i \subset T$.

Definition 2.24. The comb representation of an ordered triangulation (X, Ψ) is a set of combs $X_c = (C(T_1, h_1), C(T_2, h_2), ..., C(T_n, h_n))$ such that for $i, j \in \{0, 1, 2, 3\}$, $(T, h), (T', h') \in X$, we join by a line the spike i of $C(T, h)$ to the spike j of $C(T', h')$ if $x_i(T) = x_j(T')$.

Remark 2.25. Since we can work out from a triangulation which points are regular, ideal and hyperideal by looking at the induced triangulation on the boundary of the neighbourhoods of each vertex, we do not need to specify this typology of vertices in the comb representation for the representation to define an ordered ideal triangulation of a manifold.

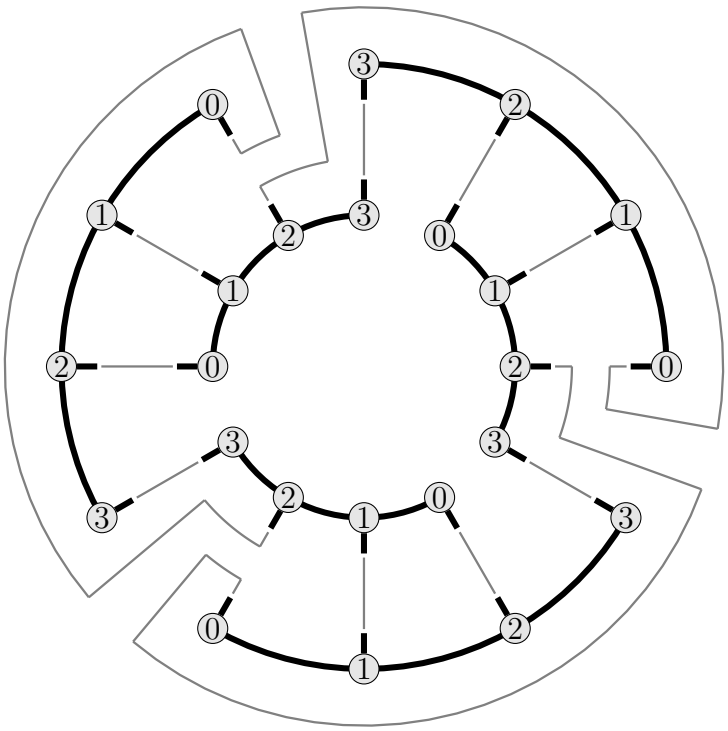

Figure 2.10: Comb representation of $\mathcal{T}_2$.

Remark 2.26. As we can see in Figure 2.10 for the triangulation $\mathcal{T}_2$ of M_2, the comb representation is a compact of representing all the information needed to reconstruct the ideal ordered triangulation $\mathcal{T} = (X, \Psi, I, H)$.

Chapter 3

The hyperbolic volume

Let $\mathbb{H}^3$ denote the hyperbolic 3-space.

Let M be a 3-manifold with boundary which admits an ideal triangulation $\mathcal{T} = (X, \Psi, I, H)$. We give M a complete hyperbolic structure (unique up to isometry) by constructing a hyperbolic structure on each tetrahedra of $\mathcal{T}$. This will enable us to use a volume formula made by Ushijima, that computes the hyperbolic volumes of the tetrahedra of $\mathcal{T}$ by using their dihedral angles. Hence, we will get the hyperbolic volume of M given its geometric angle structure and apply this to M_2 and M_3.

3.1 Hyperbolic structure on M

Let M be a 3-manifold with boundary which admits an ideal triangulation $\mathcal{T} = (X, \Psi, I, H)$.

Definition 3.1 (Frigerio, Section 1, [5])**.** Let M be a compact 3-manifold with boundary $\partial M = \partial M_1 \cup \partial M_2 \cup ... \cup \partial M_{p+q}$ which has for $k \in \{1, ..., p\}$, ∂M_k homeomorphic to $S^1 \times S^1$ and for $k \in \{p+1, ..., p+q\}$, ∂M_k homeomorphic to Σ_{g_k} for some $g_k \in \mathbb{N}_{\geq 2}$. We say that M is hyperbolic if $M \setminus \{\partial M_1 \cup \partial M_2 \cup ... \cup \partial M_p\}$ is a complete finite-volume hyperbolic 3-manifold with geodesic boundary.

Remark 3.2. Mostow-Prasad's rigidity theorem, first stated in [10], states that for any two hyperbolic manifolds M and M' that are homotopically equivalent, then M and M' are isometric. In particular, any two complete hyperbolic structures on M are isometric. Thus, for M hyperbolic, the hyperbolic structure on $M \setminus \{\partial M_1 \cup \partial M_2 \cup ... \cup \partial M_p\}$ is unique up to isometry.

Definition 3.3 (Frigerio, Section 2, [5])**.** Let $(T,h) \in X$. We define the set of *ideal vertices* of (T,h) as

$$I_T := \left\{ v_i \;\middle|\; \begin{array}{l} i \in \{0,1,2,3\}, \\ v_i \in \nu \text{ such that } \nu \in I \end{array} \right\},$$

and we define the set of *hyperideal vertices* of (T,h) as

$$H_T := \left\{ v_i \;\middle|\; \begin{array}{l} i \in \{0,1,2,3\} \\ v_i \in \nu \text{ such that } \nu \in H \end{array} \right\}.$$

A *partial truncation* of a tetrahedron (T,h) is defined as a pair (T^*,h^*) where $T^* = T \setminus \{I_T \cup U_{H_T}\}$ and $h^* = (h^{-1}|_{T^*})^{-1}$ where U_{H_T} denote a small open neighbourhood in T of the vertices in H_T, i.e the hyperideal vertices. For a face $f \subset T$, we define the associated *lateral hexagon* of T^* as $f^* := f \cap T^*$. For a hyperideal vertex $v \in H_T$, we define the associated *truncation triangle* of T^* as $v^* = \partial U_v \cap T^*$ where U_v denotes the component of U_{H_T} which is the open neighbourhood in T of v.

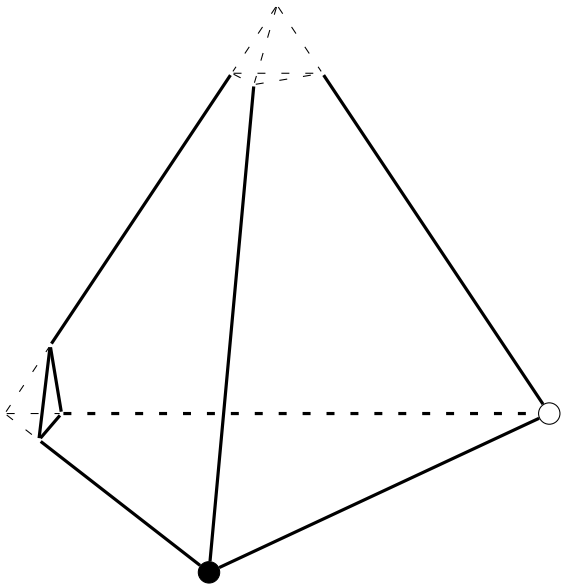

Figure 3.1: The partial truncation of (T,h) where the left vertex is hyperideal, the bottom one is regular and the top and right one are ideal.

Example 3.4. In Figure 3.1, we truncated a closed neighbourhood of the top vertex, but this is topologically equivalent to removing a point, as it is done for the right vertex. Those two cases are ideal.

Definition 3.5. An *angle structure on a tetrahedron* (T,h) is a 6-tuple $\alpha_T = (A,B,C,D,E,F)$ of interior dihedral angles $A,B,C,D,E,F \in [0,\pi]$, such that the dihedral angle of e_{01} (respectively, e_{02}, e_{03}, e_{12}, e_{13}, e_{23}) is E (respectively D, C, F, A, B) (as in Figure 3.2). An *angle structure on a triangulation* (X,Ψ) is a set $\alpha = \{\alpha_T \,|\, (T,h) \in X\}$.

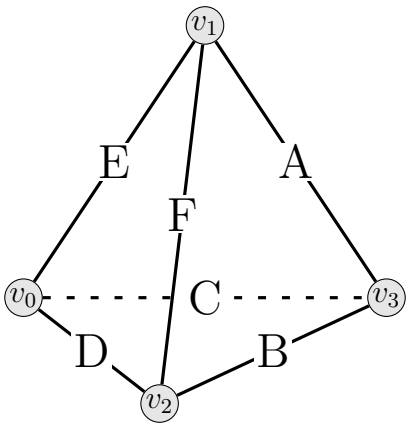

Figure 3.2: The configuration of dihedral angles on (T, h).

Remark 3.6. Given a triangulation $\mathcal{T}$, we wish to give to the partial truncations of each tetrahedron hyperbolic structures such that they match under $\sim$ in order to construct a complete hyperbolic structure on M. When given an hyperbolic structure, each partially truncated tetrahedron has dihedral angles defined at each edge. In order to have this complete hyperbolic structure on M, one can derive equations that these angles have to satisfy. Those are named the edge gluing and completeness equations and are derived in [12, Section 4.2 and 4.3].

Definition 3.7. Let M be an hyperbolic compact 3-manifold with boundary that admits an ideal triangulation $\mathcal{T} = (X, \Psi, I, H)$. We say that $\mathcal{T}$ is *geometric* if (X, Ψ) admits an angle structure satisfying the edge gluing and completeness equations and all dihedral angles are non zero. We call such an angle structure, a *geometric angle structure*.

Definition 3.8 (Frigerio, Section 2, [5])**.** Let $\mathcal{T} = (X, \Psi, I, H)$ be a geometric ideal triangulation and $(T, h) \in X$ a tetrahedron of $\mathcal{T}$. A *geometrical realization* of a tetrahedron (T, h) is defined as an embedding in $\mathbb{H}^3$ of its associated partial truncation (T^*, h^*) such that the truncation triangles are geodesic triangles, the lateral hexagons are geodesic polygons, adjacent truncation triangles and lateral hexagons lie at right angle to each other and the dihedral angles are given by a geometric angle structure on $\mathcal{T}$.

Remark 3.9. We state that a geometric realization of a tetrahedron (T, h) of a triangulation $\mathcal{T}$ is a generalized hyperbolic tetrahedron (see [13, Definition 3.1]). In next section, we give a volume formula for generalized hyperbolic tetrahedra. However, we will only apply this formula for geometric realizations in this thesis. Thus, from now on, when we refer to generalized hyperbolic tetrahedra, think of a geometric realization.

3.2 The volume formula for generalized hyperbolic tetrahedra

In [13], Ushijima gives a volume formula for generalized hyperbolic tetrahedra with a given angle structure. Recall that the geometric realization of the tetrahedron (T, h) of a triangulation $\mathcal{T}$ is a specific case of generalized hyperbolic tetrahedron. Hence, we can use Theorem 3.10 to compute the hyperbolic volumes of the geometric realizations of the tetrahedra of a triangulation.

Let $T = T(A, B, C, D, E, F)$ be a generalized tetrahedron in the hyperbolic space $\mathbb{H}^3$ (see [13, Definition 3.1]) whose angle structure is as in Figure 3.2.

Let G be :

$$G = \begin{pmatrix} 1 & -\cos A & -\cos B & -\cos F \\ -\cos A & 1 & -\cos C & -\cos E \\ -\cos B & -\cos C & 1 & -\cos D \\ -\cos F & -\cos E & -\cos D & 1 \end{pmatrix}.$$

Let $Li_2(z)$ be the dilogarithm function defined in [13, Introduction] by the analytic continuation of the following integral:

$$Li_2(x) := -\int_0^x \frac{\log(1-t)}{t} \mathrm{d}t \quad \text{for } x \in \mathbb{R}_{>0}.$$

Let I be the principal square root of -1 , $a := \exp(I \cdot A)$, $b := \exp(I \cdot B)$, ..., $F := \exp(I \cdot F)$ and let $U(z, T)$ be the complex valued function defined as follows:

$$\begin{aligned} U(z,T) := \frac{1}{2}(&Li_2(z) + Li_2(abdez) + Li_2(acdfz) + Li_2(bcefz) \\ &- Li_2(-abcz) - Li_2(-aefz) - Li_2(-bdfz) - Li_2(-cdez)). \end{aligned}$$

We denote by z_1 and z_2 the two complex numbers defined as follows:

$$\begin{aligned} z_1 &:= -2\frac{\sin A \sin D + \sin B \sin E + \sin C \sin F - \sqrt{\det G}}{ad + be + cf + abf + ace + bcd + def + abcdef}, \\ z_2 &:= -2\frac{\sin A \sin D + \sin B \sin E + \sin C \sin F + \sqrt{\det G}}{ad + be + cf + abf + ace + bcd + def + abcdef}, \end{aligned}$$

where $\sqrt{\det G} \in I\mathbb{R}_{>0}$ is the principal square root of $\det G$.

Theorem 3.10 (Ushijima, Theorem 1.1, [13])**.** *The hyperbolic volume $Vol_H(T)$ of a generalized tetrahedron $T = T(A, B, C, D, E, F)$ is given as follows:*

$$Vol_H(T) = \frac{1}{2}\mathcal{I}(U(z_1, T) - U(z_2, T)),$$

where $\mathcal{I}$ means the imaginary part.

Remark 3.11. Let M be an hyperbolic compact 3-manifold with boundary that admits a geometric ideal triangulation $\mathcal{T} = (X, \Psi, I, H)$. From Theorem 3.10, we have that, given its geometric angle structure, we can compute the hyperbolic volumes of the geometric realizations of the tetrahedra of $\mathcal{T}$. This enables us to compute the hyperbolic volume $Vol_H(M)$ of M, as the sum of the hyperbolic volumes of the tetrahedra of $\mathcal{T}_g$.

3.3 Applying the volume formula on the geometric realization of the ideal triangulation $\mathcal{T}_g$ of M_g

Let $g \in \mathbb{N}_{\geq 2}$. In [5, Section 2], Frigerio describes the complete hyperbolic structure on M_g by finding explicitly a geometric angle structure (see Definition 3.7) on the ideal triangulation $\mathcal{T}_g$. Hence, we have that M_g is hyperbolic and its ideal triangulation $\mathcal{T}_g = (X_g, \Psi_g, I_g, H_g)$ is geometric which allows us to compute the hyperbolic volume $Vol_H(M_g)$ given by

$$Vol_H(M_g) = \sum_{(T_g, h_g) \in X_g} Vol_H(T_g),$$

where the hyperbolic volumes $Vol_H(T_g)$ are given by Theorem 3.10 and the dihedral angles of the geometric angle structure. This computation is done in details in Section 6.1.

Setting $\alpha_2 = \frac{\pi}{6}$, $\beta_2 = 2\alpha_2$, $\gamma_2 = \arccos((2\cos\alpha_2)^{-1})$ and $\delta_2 = \pi - 2\gamma_2$, Frigerio's geometric angle structure on $\mathcal{T}_2$ is as in Figure 3.3. In each column of Figure 3.3, the angle structure of each tetrahedron is the same.

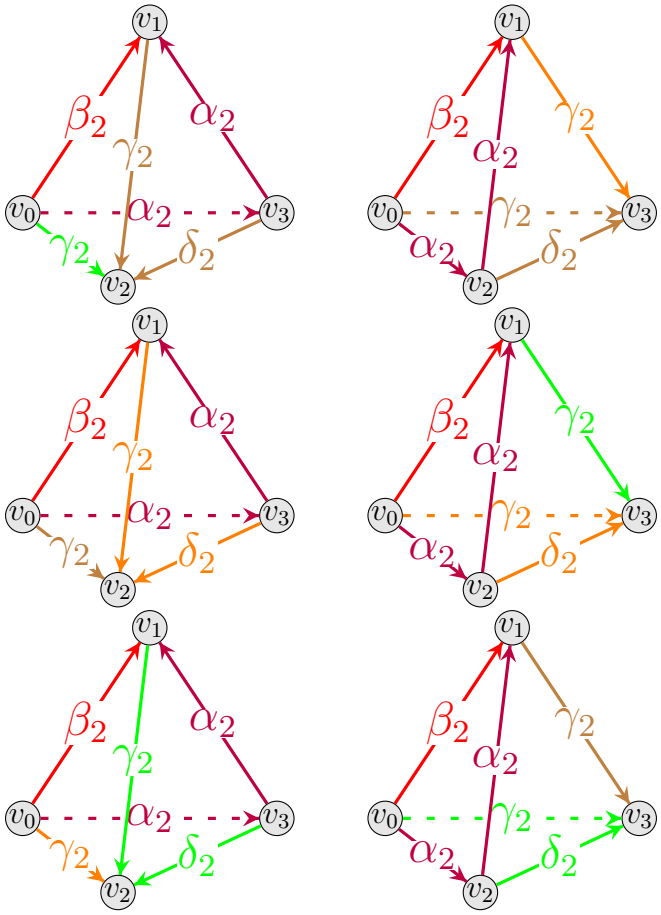

Figure 3.3: Frigerio's angle structure on $\mathcal{T}_2$

Chapter 4

Turaev-Viro Invariants

We will mostly follow the notations, conventions and definitions of [3, Section 2].

In this chapter, let us fix a pair $(r, s) \in \mathbb{N}^2$ such that $r \geq 3$ and $s \geq 1$. For such a pair (r, s), we shall first define an admissible colouring c at level r of an hyperbolic compact 3-manifold M with boundary that admits an ideal triangulation $\mathcal{T} = (X, \Psi, I, H)$. Then, we will define a Turaev-Viro type invariant $TV_{r,s}$ for $(M, \mathcal{T})$ and apply that definition to the pairs $(M_2, \mathcal{T}_2)$ and $(M_3, \mathcal{T}_3)$ defined in Section 2.2.

Notation. Let $\frac{\mathbb{N}}{2} = \left\{0, \frac{1}{2}, 1, \frac{3}{2}, ...\right\}$ the set of non-negative half integers.

Let $\frac{\mathbb{N}_{odd}}{2} = \left\{\frac{1}{2}, \frac{3}{2}, \frac{5}{2}, ...\right\}$ denote the set of non-negative half-odd-integers.

Let I_r denote the subset $\left\{0, \frac{1}{2}, 1, ..., \frac{r-2}{2}\right\}$ of $\frac{\mathbb{N}}{2}$. For example, $I_3 = \left\{0, \frac{1}{2}\right\}$ and $I_4 = \left\{0, \frac{1}{2}, 1\right\}$.

Let $I = \sqrt{-1}$ be the principal square root of -1 and as a convention, we let $\sqrt{-x} = I\sqrt{x}$ for $x \geq 0$.

4.1 Admissible colourings

4.1.1 Definition

Definition 4.1. A triple (i, j, k) of elements of I_r is called *admissible* if it satisfies the following conditions:

(i) a) $i + j \geq k$,

b) $j + k \geq i$,

c) $k + i \geq j$,

(ii) $i + j + k \in \mathbb{N}$,

(iii) $i + j + k \leq r{-}2$.

Remark 4.2. Definition 4.1 does not depend on the order of the elements of the triple.

Lemma 4.3. *Let $i, k \in I_r$. Then (i, i, k) is admissible if and only if $k \in \mathbb{N}$ and $\frac{k}{2} \leq i \leq \frac{r-2-k}{2}$.*

Proof. Let $i, k \in I_r$. By Definition 4.1, (i, i, k) is admissible if it satisfies the following conditions:

(i) a) $2i \geq k$,

b) $i + k \geq i$,

c) $k + i \geq i$,

(ii) $2i + k \in \mathbb{N}$,

(iii) $2i + k \leq r{-}2$.

Conditions (ib) and (ic) are satisfied for all $i, k \in I_r$ since $(k \in I_r \implies k \geq 0)$.

Condition (ii) is satisfied if and only if $k \in \mathbb{N}$, since $\big(i \in I_r \subset \frac{\mathbb{N}}{2} \implies 2i \in \mathbb{N}\big)$.

Taken together, conditions (ia) and (iii) are equivalent to the following condition:

$k \leq 2i \leq r{-}2{-}k$, i.e $\frac{k}{2} \leq i \leq \frac{r-2-k}{2}$.

We conclude that (i, i, k) satisfies the conditions of admissibility if and only if $k \in \mathbb{N}$ and $\frac{k}{2} \leq i \leq \frac{r-2-k}{2}$. □

Lemma 4.4. *Let $i, j, k, l, m \in I_r$ such that (i, j, k) and (k, l, m) are admissible. Then, $i + j + l + m \in \mathbb{N}$.*

Proof. Let $i, j, k, l, m \in I_r$ such that (i, j, k) and (k, l, m) are admissible. Then, by condition (ii) of Definition 4.1, we have that $i + j + k \in \mathbb{N}$ and $k + l + m \in \mathbb{N}$, thus $i + j + 2k + l + m \in \mathbb{N}$. Since $k \in I_r$, $2k \in \mathbb{N}$, we conclude that $i + j + l + m \in \mathbb{N}$. □

Lemma 4.5. *Let $i, j, k \in I_r$ such that $k \in \mathbb{N}$. Then the following conditions are equivalent:*

(i) $i + j + k \in \mathbb{N}$,

(ii) $i + j \in \mathbb{N}$,

(iii) either $i, j \in \mathbb{N}$ *or* $i, j \in \frac{\mathbb{N}_{odd}}{2}$.

Remark 4.6. This lemma can be applied to condition (ii) of Definition 4.1 when i, j or $k \in \mathbb{N}$.

Proof. Let $i, j, k \in I_r$ such that $k \in \mathbb{N}$.

$(i) \iff (ii)$ is immediate since $k \in \mathbb{N}$.

$(ii) \iff (iii)$: If $i + j \in \mathbb{N}$, then $(i \in \mathbb{N} \iff j \in \mathbb{N})$ and $\left(i \in \frac{\mathbb{N}_{odd}}{2} \iff j \in \frac{\mathbb{N}_{odd}}{2}\right)$.

Reciprocally, if either $i, j \in \mathbb{N}$ or $i, j \in \frac{\mathbb{N}_{odd}}{2}$, then $i + j \in \mathbb{N}$.

Hence, the three conditions are equivalent. □

Definition 4.7. Let M be an hyperbolic compact 3-manifold with boundary that admits an ideal triangulation $\mathcal{T} = (X, \Psi, I, H)$ (see Definition 2.13). A *colouring at level r of $(M, \mathcal{T})$* is an application $c : X^1_\sim \to I_r$. The colouring c is called *admissible* if for every $(T, h) \in X$, the triples $(c([e_{01}]), c([e_{02}]), c([e_{03}]))$, $(c([e_{01}]), c([e_{12}]), c([e_{13}]))$, $(c([e_{02}]), c([e_{12}]), c([e_{23}]))$ and $(c([e_{03}]), c([e_{13}]), c([e_{23}]))$ are admissible where $[e_{kl}] \in X^1_\sim$ denote the equivalence class under $\sim$ of the edge e_{kl} of (T, h) for $k, l \in \{0, 1, 2, 3\}$ such that $k \neq l$.

4.1.2 Admissible colourings of $(M_2, \mathcal{T}_2)$

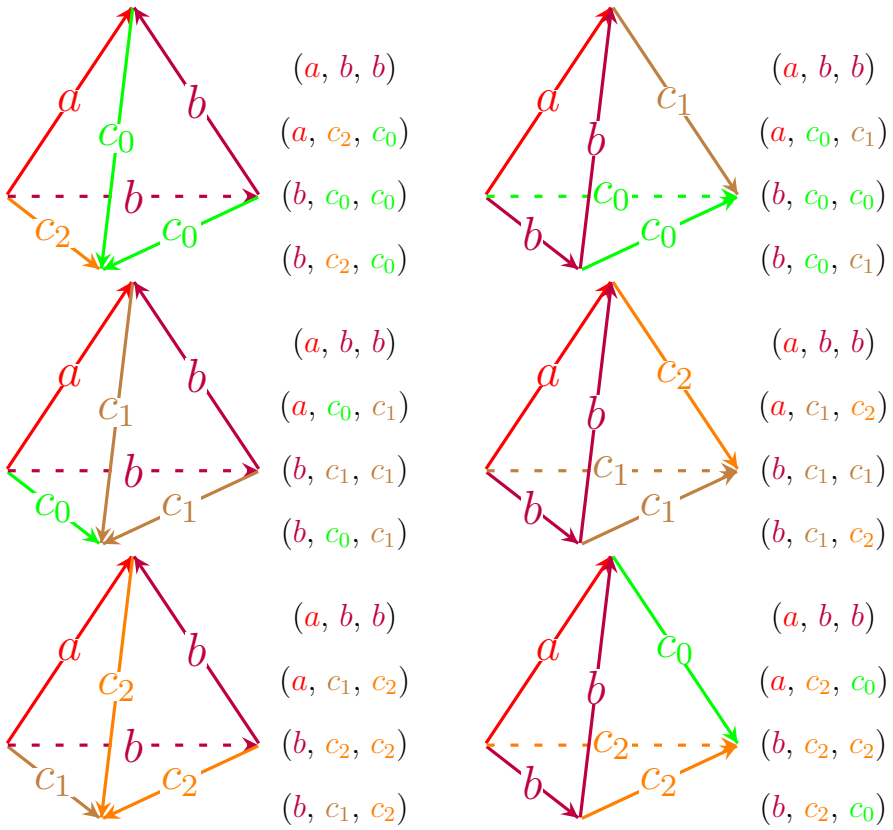

Figure 4.1: A general colouring c at level r of the ideal tetrahedra of $\mathcal{T}_2$ together with their respective triples that need to be admissible in order for c to be admissible

Let (a, b, c_0, c_1, c_2) be a 5-tuple of elements of I_r. Let $c : X^1_\sim \to I_r$ be a colouring at level r of $(M_2, \mathcal{T}_2)$ such as in Figure 4.1. By Definition 4.7, for c to be admissible, we need the following triples of elements of I_r to be admissible:

$$\begin{array}{llll} (a,b,b), & (a,c_2,c_0), & (b,c_2,c_2), & (b,c_2,c_0), \\ & (a,c_0,c_1), & (b,c_0,c_0), & (b,c_0,c_1), \\ & (a,c_1,c_2), & (b,c_1,c_1), & (b,c_1,c_2). \end{array}$$

4.1.3 Admissible colourings of $(M_3, \mathcal{T}_3)$

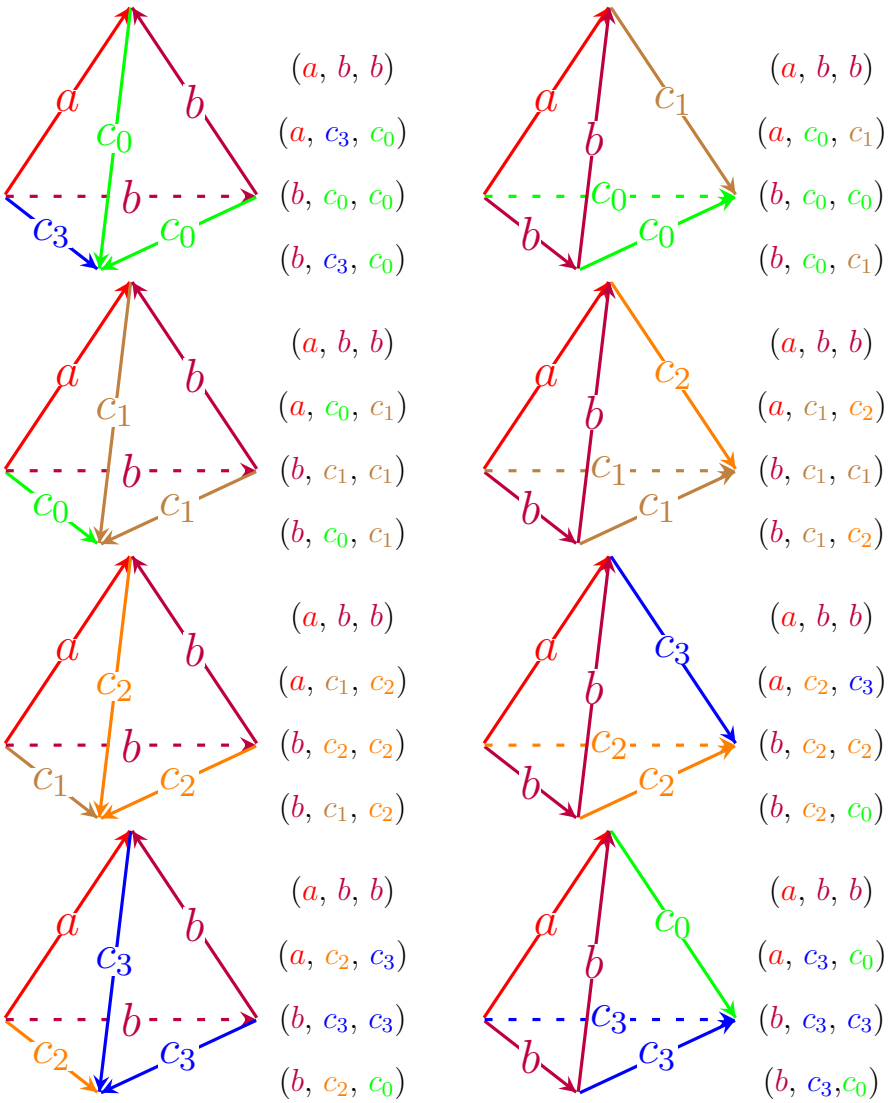

Figure 4.2: A general colouring c at level r of the ideal tetrahedra of $\mathcal{T}_3$ together with their respective triples that need to be admissible in order for c to be admissible

Let $(a, b, c_0, c_1, c_2, c_3)$ be a 6-tuple of elements of I_r. Let $c : X^1_\sim \to I_r$ be a colouring at level r of $(M_3, \mathcal{T}_3)$ such as in Figure 4.2. By Definition 4.7, for c to be admissible, we need the following triples of elements of I_r to be admissible:

$$
\begin{array}{llll}
(a,b,b), & (a,c_3,c_0), & (b,c_3,c_3), & (b,c_3,c_0),\\
 & (a,c_0,c_1), & (b,c_0,c_0), & (b,c_0,c_1),\\
 & (a,c_1,c_2), & (b,c_1,c_1), & (b,c_1,c_2),\\
 & (a,c_2,c_3), & (b,c_2,c_2), & (b,c_2,c_3).
\end{array}
$$

4.1.4 Admissible colourings of $(M_g, \mathcal{T}_g)$

Let $g \in \mathbb{N}_{\geq 2}$. For a general colouring c at level r of $(M_g, \mathcal{T}_g)$, similar as in Figures 4.1 and 4.2, to be admissible, we need the following triples of elements of I_r to be admissible:

$$\begin{array}{cccc} (a,b,b), & (a,c_g,c_0), & (b,c_g,c_g), & (b,c_g,c_0), \\ \text{and for all } i \in \{0,1,2,...,g-1\}, & (a,c_i,c_{i+1}), & (b,c_i,c_i), & (b,c_i,c_{i+1}). \end{array}$$

These admissibility conditions can be rewritten as stated in the next proposition.

Proposition 4.8. *Let a, b, c_0, c_1, c_2, ..., $c_g \in I_r$.*

The conditions (A), (B), (C), (D), (E), (F) and (G) defined below are simultaneously satisfied if and only if the conditions (1), (2), (3), (4), (5) and (6) defined below are simultaneously satisfied.

The conditions (A), (B), (C), (D), (E), (F) and (G) are written:

(A) (a,b,b) is admissible,

(B) (a,c_g,c_0) is admissible,

(C) (b,c_g,c_g) is admissible,

(D) (b,c_g,c_0) is admissible,

(E) $\forall i \in \{0,1,2,...,g-1\}$, (a,c_i,c_{i+1}) is admissible,

(F) $\forall i \in \{0,1,2,...,g-1\}$, (b,c_i,c_i) is admissible,

(G) $\forall i \in \{0,1,2,...,g-1\}$, (b,c_i,c_{i+1}) is admissible,

The conditions (1), (2), (3), (4), (5) and (6) are written:

(1) $a \in \mathbb{N}$,

(2) $b \in \mathbb{N}$,

(3) either $\forall i \in \{0,1,2...,g\}$, $c_i \in \mathbb{N}$ or $\forall i \in \{0,1,2,...,g\}$, $c_i \in \frac{\mathbb{N}_{odd}}{2}$,

(4) $\frac{a}{2} \leq b \leq \frac{r-2-a}{2}$,

(5) *a)* $\forall i \in \{0, 1, 2..., g-1\}$, $\frac{b}{2} \leq c_{i+1} \leq \frac{r-2-b}{2}$,

b) $\forall i \in \{0, 1, 2..., g-1\}$, $a - c_i \leq c_{i+1} \leq r - 2 - a - c_i$,

c) $\forall i \in \{0, 1, 2..., g-1\}$, $c_i - a \leq c_{i+1} \leq a + c_i$,

d) $\forall i \in \{0, 1, 2..., g-1\}$, $c_i - b \leq c_{i+1} \leq b + c_i$,

(6) *a)* $\frac{b}{2} \leq c_0 \leq \frac{r-2-b}{2}$,

b) $a - c_g \leq c_0 \leq r - 2 - a - c_g$,

c) $c_g - a \leq c_0 \leq a + c_g$,

d) $c_g - b \leq c_0 \leq b + c_g$.

Proof. Let a, b, c_0, c_1, c_2, ..., $c_g \in I_r$.

Step 1 : $(A) \iff (1) \wedge (4)$;

This step follows immediately from Lemma 4.3.

Step 2 : $(A) \wedge (E) \iff (1) \wedge (3) \wedge (4) \wedge (5b) \wedge (5c)$;

By Definition 4.1, Condition (E) is equivalent to the following conditions :

(Ei) (a) $\forall i \in \{0, 1, 2..., g-1\}$, $c_i + c_{i+1} \geq a$,

(b) $\forall i \in \{0, 1, 2..., g-1\}$, $c_i + a \geq c_{i+1}$,

(c) $\forall i \in \{0, 1, 2..., g-1\}$, $a + c_{i+1} \geq c_i$,

(Eii) $\forall i \in \{0, 1, 2..., g-1\}$, $c_i + c_{i+1} + a \in \mathbb{N}$,

(Eiii) $\forall i \in \{0, 1, 2..., g-1\}$, $c_i + c_{i+1} + a \leq r-2$.

To prove Step 2, we first remark that:

$$(Eia) \wedge (Eiii) \iff (5b),$$
$$(Eib) \wedge (Eic) \iff (5c).$$

It remains to prove that :

$$(A) \wedge (Eii) \iff (1) \wedge (3) \wedge (4).$$

It follows from Step 1 that :

$$(A) \wedge (Eii) \iff (1) \wedge (4) \wedge (Eii).$$

From Lemma 4.5, it follows that

$$(1)\wedge(4)\wedge(Eii) \iff (1)\wedge(4)\wedge\left(\forall i \in \{0,1,2...,g-1\}, (c_i, c_{i+1} \in \mathbb{N}) \vee \left(c_i, c_{i+1} \in \frac{\mathbb{N}_{odd}}{2}\right)\right).$$

Finally, it follows by a quick induction that:

$$(1)\wedge(4)\wedge\left(\forall i \in \{0,1,2...,g-1\}, (c_i, c_{i+1} \in \mathbb{N}) \vee \left(c_i, c_{i+1} \in \frac{\mathbb{N}_{odd}}{2}\right)\right) \iff (1)\wedge(4)\wedge(3).$$

Step 3 : $(A) \wedge (B) \wedge (E) \iff (1) \wedge (3) \wedge (4) \wedge (5b) \wedge (5c) \wedge (6b) \wedge (6c)$;

From Step 2, it follows that:

$$(A) \wedge (E) \iff (1) \wedge (3) \wedge (4) \wedge (5b) \wedge (5c).$$

By Definition 4.1, Condition (B) is equivalent to the following conditions :

(Bi) a) $c_g + c_0 \geq a$,

b) $c_g + a \geq c_0$,

c) $a + c_0 \geq c_g$,

(Bii) $c_g + c_0 + a \in \mathbb{N}$,

(Biii) $c_g + c_0 + a \leq r-2$.

To prove Step 3, we first remark that:

$$(Bia) \wedge (Biii) \iff (6b),$$
$$(Bib) \wedge (Bic) \iff (6c).$$

Finally, let us prove the following implication which will imply Step 3:

$$(A) \wedge (E) \implies (Bii).$$

From Step 2, it follows that

$$(A) \wedge (E) \implies (1) \wedge (3).$$

Furthermore, using Lemma 4.5, we have that:

$$(1) \wedge (3) \implies (Bii).$$

Step 4 : $(C) \wedge (F) \iff (2) \wedge (5a) \wedge (6a)$;

This step follows immediately from Lemma 4.3.

Step 5 : $(A) \wedge (B) \wedge (C) \wedge (E) \wedge (F) \wedge (G) \iff$
$(1) \wedge (2) \wedge (3) \wedge (4) \wedge (5a) \wedge (5b) \wedge (5c) \wedge (5d) \wedge (6a) \wedge (6b) \wedge (6c)$;

From Step 3, it follows that:

$$(A) \wedge (B) \wedge (E) \iff (1) \wedge (3) \wedge (4) \wedge (5b) \wedge (5c) \wedge (6b) \wedge (6c).$$

From Step 4, it follows that:

$$(C) \wedge (F) \iff (2) \wedge (5a) \wedge (6a).$$

By Definition 4.1, Condition (G) is equivalent to the following conditions :

(Gi) a) $\forall i \in \{0, 1, 2..., g-1\}$, $c_i + c_{i+1} \geq b$,

b) $\forall i \in \{0, 1, 2..., g-1\}$, $c_i + b \geq c_{i+1}$,

c) $\forall i \in \{0, 1, 2..., g-1\}$, $b + c_{i+1} \geq c_i$,

(Gii) $\forall i \in \{0, 1, 2..., g-1\}$, $c_i + c_{i+1} + b \in \mathbb{N}$,

(Giii) $\forall i \in \{0, 1, 2..., g-1\}$, $c_i + c_{i+1} + b \leq r-2$.

Following what precedes, in order to prove Step 5, we only need to prove that:

Step 5.1 $(C) \wedge (F) \implies (Gia) \wedge (Giii)$,

Step 5.2 $(Gib) \wedge (Gic) \iff (5d)$,

Step 5.3 $(A) \wedge (E) \implies (Gii)$.

Let us prove Step 5.1. From Step 4, it follows that

$$(C) \wedge (F) \implies (5a) \wedge (6a).$$

Furthermore, we have by adding inequalities that :

$$(5a) \wedge (6a) \implies (Gia) \wedge (Giii).$$

Step 5.2 follows immediately from the definitions.

Finally, let us prove Step 5.3. From Step 2, it follows that

$$(A) \wedge (E) \implies (1) \wedge (3).$$

Furthermore, using Lemma 4.5, we have that:

$$(1) \wedge (3) \implies (Gii).$$

This concludes the proof of Step 5.

Step 6 : $(A) \wedge (B) \wedge (C) \wedge (D) \wedge (E) \wedge (F) \wedge (G) \iff$
$(1) \wedge (2) \wedge (3) \wedge (4) \wedge (5a) \wedge (5b) \wedge (5c) \wedge (5d) \wedge (6a) \wedge (6b) \wedge (6c) \wedge (6d)$;

We prove Step 6 almost exactly as we proved Step 5. The only difference being the (G) conditions become (D) conditions and $(5d)$ becomes $(6d)$.

This concludes the proof of the proposition. □

4.2 Turaev-Viro Invariants

Recall that, at the beginning of this chapter, we fixed $(r, s) \in \mathbb{N}^2$ such that $r \geq 3$ and $s \geq 1$.

4.2.1 Quantum $6j$-symbols

Definition 4.9 (Quantum number)**.** For $n \in \mathbb{N}$, the *quantum number* $[n]$ is the real number defined by

$$[n] := \frac{\sin\left(\frac{ns\pi}{r}\right)}{\sin\left(\frac{s\pi}{r}\right)} \in \mathbb{R}.$$

Remark 4.10. Note that $[r] = \frac{\sin(s\pi)}{\sin\left(\frac{s\pi}{r}\right)} = 0$ and $\lim\limits_{r\to\infty} \frac{\sin\left(\frac{ns\pi}{r}\right)}{\sin\left(\frac{s\pi}{r}\right)} = n$.

Definition 4.11 (Quantum factorial)**.** For $n \in \mathbb{N}$, the *quantum factorial* $[n]!$ is defined by

$$[n]! := [n][n-1]...[2][1] \in \mathbb{R}$$

and, as a convention, $[0]! = 1$.

Remark 4.12. Note that for $n \geq r$, $[n]! = 0$ and for $n \leq r-1$, $[n]! \neq 0$.

Definition 4.13. For an admissible triple (i, j, k) of elements of I_r, we define

$$\Delta(i, j, k) := \sqrt{\frac{[i+j-k]![i-j+k]![-i+j+k]!}{[i+j+k+1]!}}.$$

Recall that as a convention, we let $\sqrt{-x} = I\sqrt{x}$ for I the principal square root of -1 and $x \geq 0$.

Remark 4.14. Note that condition (iii) of Definition 4.1 ensures that $i+j+k+1 \leq r-1$, thus $[i+j+k+1]! \neq 0$.

Definition 4.15 (Quantum 6j-symbols)**.** Let (i,j,k,l,m,n) be a 6-tuple of elements of I_r such that (i,j,k), (j,l,n), (i,m,n) and (k,l,m) are admissible.

Let $T_1 = i+j+k$, $T_2 = j+l+n$, $T_3 = i+m+n$, $T_4 = k+l+m$, $Q_1 = i+j+l+m$, $Q_2 = i+k+l+n$ and $Q_3 = j+k+m+n$.

Then *the quantum 6j-symbol* for the 6-tuple (i,j,k,l,m,n) is defined by

$$\begin{vmatrix} i & j & k \\ l & m & n \end{vmatrix} := \sqrt{-1}^{-2(i+j+k+l+m+n)} \Delta(i,j,k)\Delta(j,l,n)\Delta(i,m,n)\Delta(k,l,m) \cdot \sum_{z=\max\{T_1,T_2,T_3,T_4\}}^{\min\{Q_1,Q_2,Q_3\}} \frac{(-1)^z [z+1]!}{[z-T_1]![z-T_2]![z-T_3]![z-T_4]![Q_1-z]![Q_2-z]![Q_3-z]!}$$

.

Remark 4.16. Note that $T_1, T_2, T_3, T_4 \in \mathbb{N}$ because of condition (ii) of Definition 4.1. Since (i,j,k) and (k,l,m) are admissible, $Q_1 \in \mathbb{N}$ by Lemma 4.4. Since (i,j,k) and (j,l,n) are admissible, $Q_2 \in \mathbb{N}$ by Lemma 4.4. Since (i,j,k) and (i,m,n) are admissible, $Q_3 \in \mathbb{N}$ by Lemma 4.4. Since (k,l,m) is admissible, by condition (i) of Definition 4.1, $l+m \geq k$, thus $Q_1 \geq T_1$. Since (i,m,n) is admissible, by condition (i) of Definition 4.1, $m+i \geq n$, thus $Q_1 \geq T_2$. Since (j,l,n) is admissible, by condition (i) of Definition 4.1, $j+l \geq n$, thus $Q_1 \geq T_3$. Since (i,j,k) is admissible, by condition (i) of Definition 4.1, $i+j \geq k$, thus $Q_1 \geq T_4$. Thus, $Q_1 \geq \max\{T_1,T_2,T_3,T_4\}$. Similar reasoning ensures that $Q_2 \geq \max\{T_1,T_2,T_3,T_4\}$ and $Q_3 \geq \max\{T_1,T_2,T_3,T_4\}$. We ensure thus that $\min\{Q_1,Q_2,Q_3\} \geq \max\{T_1,T_2,T_3,T_4\}$ and that the sum in Definition 4.15 is well-defined.

Proposition 4.17 (Allowed symbol permutations)**.** *Let (i,j,k,l,m,n) be a 6-tuple of elements of I_r such that (i,j,k), (j,l,n), (i,m,n), (k,l,m) are admissible.*

Then, we have the following allowed permutations:

$$\begin{vmatrix} i & j & k \\ l & m & n \end{vmatrix} = \begin{vmatrix} j & i & k \\ m & l & n \end{vmatrix} = \begin{vmatrix} i & k & j \\ l & n & m \end{vmatrix} = \begin{vmatrix} i & m & n \\ l & j & k \end{vmatrix} = \begin{vmatrix} l & m & k \\ i & j & n \end{vmatrix} = \begin{vmatrix} l & j & n \\ i & m & k \end{vmatrix}.$$

Proof. If you perform the swaps $i \leftrightarrow j$ and $l \leftrightarrow m$, then you perform the swaps $(j,l,n) \leftrightarrow (i,m,n)$ and $T_3 \leftrightarrow T_2$ in Definition 4.15. The rest isn't changed. Thus the quantum $6j$-symbol isn't changed by these two permutations and

$$\begin{vmatrix} i & j & k \\ l & m & n \end{vmatrix} = \begin{vmatrix} j & i & k \\ m & l & n \end{vmatrix}.$$

A similar reasoning gives the other allowed symbol permutations. □

Definition 4.18. For $i \in I_r$, we define $w_i := (-1)^{2i}[2i+1]$.

4.2.2 Turaev-Viro invariants of triangulated manifolds

Let M be an hyperbolic compact 3-manifold with boundary that admits an ideal triangulation $\mathcal{T} = (X, \Psi, I, H)$ (see Definition 2.13).

Definition 4.19. Let $R = X^0_\sim \setminus \{I \cup H\}$ denote the set of regular vertices. We define the *regular vertices term* as $V := \left(\sum_{i \in I_r} w_i^2\right)^{-|R|}$.

Definition 4.20. Let $c : X^1_\sim \to I_r$ be an admissible colouring at level r of $(M, \mathcal{T})$. For $\eta \in X^1_\sim$, we define the *edge term* $|\eta|_c := w_{c(\eta)}$.

Definition 4.21. Let $c : X^1_\sim \to I_r$ be an admissible colouring at level r of $(M, \mathcal{T})$. For $T \in X^3$, we define the *tetrahedron term* as

$$|T|_c = \begin{vmatrix} c([e_{01}]) & c([e_{02}]) & c([e_{12}]) \\ c([e_{23}]) & c([e_{13}]) & c([e_{03}]) \end{vmatrix},$$

where $[e_{kl}] \in X^1_\sim$ denotes the equivalence class under $\sim$ of the edge e_{kl} of T for $k, l \in \{0, 1, 2, 3\}$ such that $k \neq l$.

Definition 4.22 (Turaev-Viro invariant)**.** Let $m = |X^1_\sim|$. Let $\mathcal{A}_r(M, \mathcal{T}) = \{(c(\eta_1), ..., c(\eta_m)) \mid c : X^1_\sim \to I_r$ is an admissible colouring at level r of $(M, \mathcal{T})\}$. We define the *Turaev-Viro invariant* of M as

$$TV_{r,s}(M, \mathcal{T}) := V \sum_{(c(\eta_1),...,c(\eta_m)) \in \mathcal{A}_r(M,\mathcal{T})} \prod_{i=1}^{m} |\eta_i|_c \prod_{T \in X^3} |T|_c.$$

4.2.3 Turaev-Viro Invariant of $(M_2, \mathcal{T}_2)$

Using Definition 4.22 for $(M, \mathcal{T}) = (M_2, \mathcal{T}_2)$, which was defined in Section 2.2, we can determine the edge terms and tetrahedron terms (see Definitions 4.20 and 4.21) contributing to $TV_{r,s}(M_2, \mathcal{T}_2)$. Since there are no regular vertices in $\mathcal{T}_2$, we have that the regular vertices term $V = \left(\sum_{i \in I_r} w_i^2\right)^0 = 1$ (see Definition 4.19).

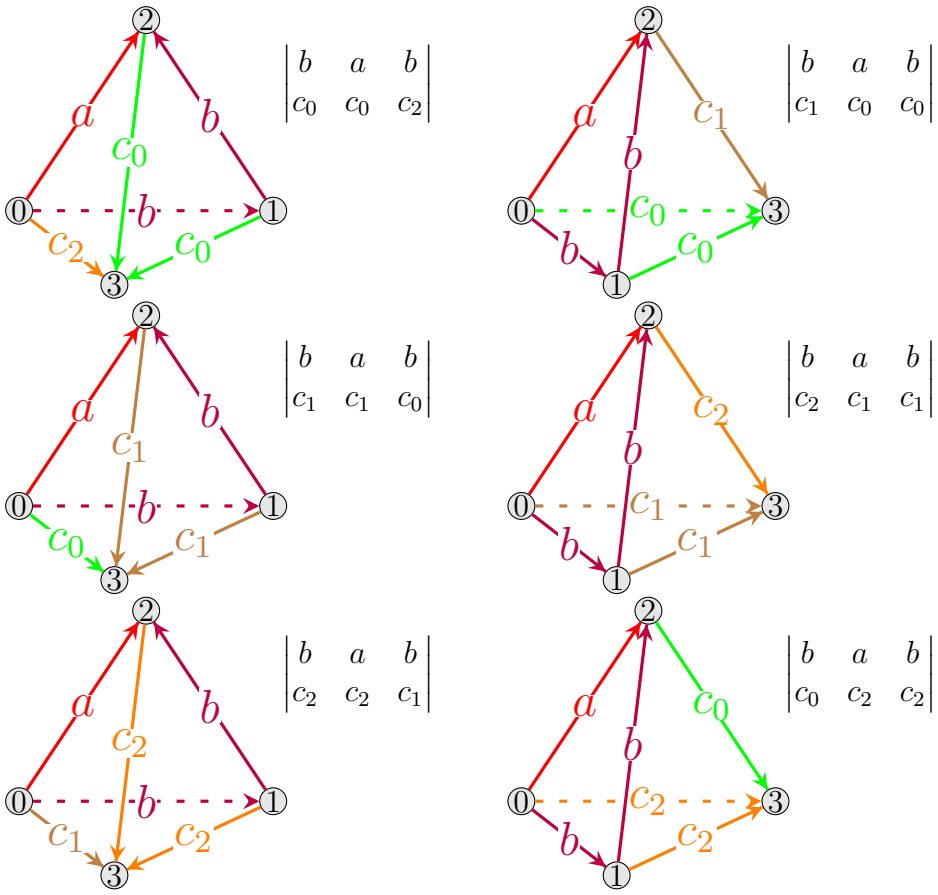

Figure 4.3: The colouring c of the ideal tetrahedra of $\mathcal{T}_2$ together with their respective tetrahedron terms

Let (a, b, c_0, c_1, c_2) be a 5-tuple of elements of I_r. A colouring $c : X^1_\sim \to I_r$ such as in Figure 4.4 is admissible if and only if it satisfies the conditions of Proposition 4.8, thus

$$\mathcal{A}_r(M_2, \mathcal{T}_2) = \left\{ (a, b, c_0, c_1, c_2) \in I_r^5 \;\middle|\; \begin{array}{l} a, b \in \mathbb{N}, \\ \frac{a}{2} \leq b \leq \frac{r-2-a}{2}, \\ \text{either } c_0, c_1, c_2 \in \mathbb{N} \text{ or } c_0, c_1, c_2 \in \frac{\mathbb{N}_{odd}}{2}, \\ \max\left(\frac{b}{2}, a - c_3, c_3 - \min(a, b)\right) \leq c_0, \\ c_0 \leq \min\left(\frac{r-2-b}{2}, r - 2 - a - c_3, \min(a, b) + c_3\right), \\ \max\left(\frac{b}{2}, a - c_0, c_0 - \min(a, b)\right) \leq c_1, \\ c_1 \leq \min\left(\frac{r-2-b}{2}, r - 2 - a - c_0, \min(a, b) + c_0\right), \\ \max\left(\frac{b}{2}, a - c_1, c_1 - \min(a, b)\right) \leq c_2, \\ c_2 \leq \min\left(\frac{r-2-b}{2}, r - 2 - a - c_1, \min(a, b) + c_1\right) \end{array} \right\}.$$

From Figure 4.4 and Definitions 4.20 and 4.21, we can determine the six tetrahedron terms $|T|_c$ and five edge terms $|\eta|_c$ associated to the colouring c which gives us the following equation:

$$TV_{r,s}(M_2,\mathcal{T}_2) = \sum_{(a,b,c_0,c_1,c_2)\in A_r(M_2,\mathcal{T}_2)} w_a w_b w_{c_0} w_{c_1} w_{c_2} \cdot \begin{vmatrix} b & a & b \\ c_0 & c_0 & c_2 \end{vmatrix} \begin{vmatrix} b & a & b \\ c_1 & c_0 & c_0 \end{vmatrix} \cdot \begin{vmatrix} b & a & b \\ c_1 & c_1 & c_0 \end{vmatrix} \begin{vmatrix} b & a & b \\ c_2 & c_1 & c_1 \end{vmatrix} \cdot \begin{vmatrix} b & a & b \\ c_2 & c_2 & c_1 \end{vmatrix} \begin{vmatrix} b & a & b \\ c_0 & c_2 & c_2 \end{vmatrix}.$$

Using Proposition 4.17 and a bit of reordering, we can rewrite the summation as:

$$TV_{r,s}(M_2,\mathcal{T}_2) = \sum_{(a,b,c_0,c_1,c_2)\in A_r(M_2,\mathcal{T}_2)} w_a w_b w_{c_0} w_{c_1} w_{c_2} \cdot \begin{vmatrix} a & b & b \\ c_0 & c_0 & c_2 \end{vmatrix} \begin{vmatrix} a & b & b \\ c_0 & c_0 & c_1 \end{vmatrix} \cdot \begin{vmatrix} a & b & b \\ c_1 & c_1 & c_0 \end{vmatrix} \begin{vmatrix} a & b & b \\ c_1 & c_1 & c_2 \end{vmatrix} \cdot \begin{vmatrix} a & b & b \\ c_2 & c_2 & c_1 \end{vmatrix} \begin{vmatrix} a & b & b \\ c_2 & c_2 & c_0 \end{vmatrix}.$$

4.2.4 Turaev-Viro Invariant of $(M_3, \mathcal{T}_3)$

Using Definition 4.22 for $(M,\mathcal{T}) = (M_3,\mathcal{T}_3)$, which was defined in Section 2.2, we can determine the edge terms and tetrahedron terms (see Definitions 4.20 and 4.21) contributing to $TV_{r,s}(M_3,\mathcal{T}_3)$. Since there are no regular vertices in $\mathcal{T}_3$, we have that the regular vertices term $V = \left(\sum_{i\in I_r} w_i^2\right)^0 = 1$ (see Definition 4.19).

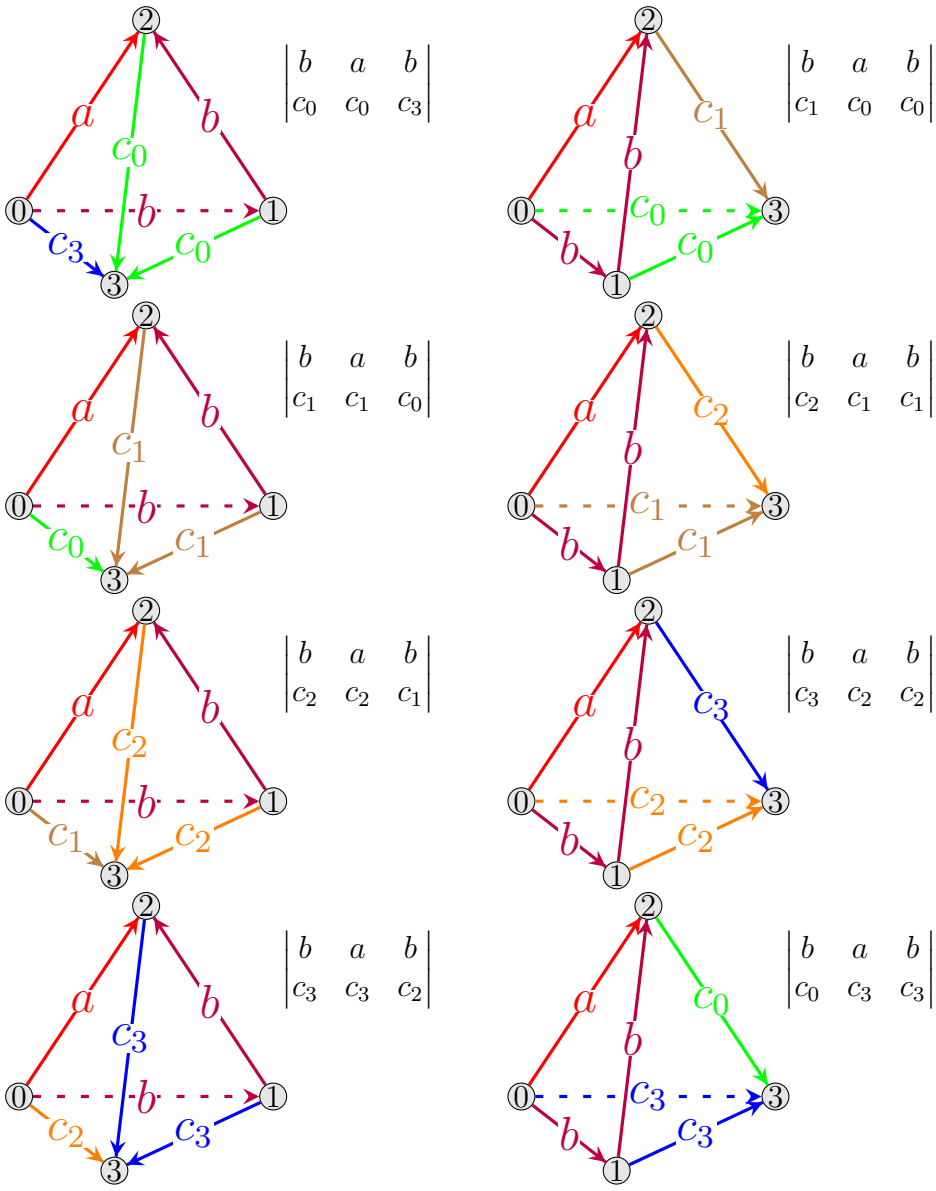

Figure 4.4: The colouring c of the ideal tetrahedra of $\mathcal{T}_3$ together with their respective tetrahedron terms

Let $(a, b, c_0, c_1, c_2, c_3)$ be a 6-tuple of elements of I_r. A colouring $c : X^1_\sim \to I_r$ such as in Figure 4.4 is admissible if and only if it satisfies the conditions of Proposition 4.8, thus

$$\mathcal{A}_r(M_3, \mathcal{T}_3) = \left\{ (a, b, c_0, c_1, c_2, c_3) \in I_r^6 \;\middle|\; \begin{array}{l} a, b \in \mathbb{N}, \\ \frac{a}{2} \leq b \leq \frac{r-2-a}{2}, \\ \text{either } c_0, c_1, c_2, c_3 \in \mathbb{N} \text{ or } c_0, c_1, c_2, c_3 \in \frac{\mathbb{N}_{odd}}{2}, \\ \max\left(\frac{b}{2}, a - c_3, c_3 - \min(a, b)\right) \leq c_0, \\ c_0 \leq \min\left(\frac{r-2-b}{2}, r - 2 - a - c_3, \min(a, b) + c_3\right), \\ \max\left(\frac{b}{2}, a - c_0, c_0 - \min(a, b)\right) \leq c_1, \\ c_1 \leq \min\left(\frac{r-2-b}{2}, r - 2 - a - c_0, \min(a, b) + c_0\right), \\ \max\left(\frac{b}{2}, a - c_1, c_1 - \min(a, b)\right) \leq c_2, \\ c_2 \leq \min\left(\frac{r-2-b}{2}, r - 2 - a - c_1, \min(a, b) + c_1\right), \\ \max\left(\frac{b}{2}, a - c_2, c_2 - \min(a, b)\right) \leq c_3, \\ c_3 \leq \min\left(\frac{r-2-b}{2}, r - 2 - a - c_2, \min(a, b) + c_2\right) \end{array} \right\}.$$

From Figure 4.4 and Definitions 4.20 and 4.21, we can determine the eight tetrahedron terms $|T|_c$ and six edge terms $|\eta|_c$ associated to the colouring c which gives us the following equation:

$$\begin{aligned} TV_{r,s}(M_3, \mathcal{T}_3) = \sum_{(a,b,c_0,c_1,c_2,c_3) \in A_r(M_3,\mathcal{T}_3)} & w_a w_b w_{c_0} w_{c_1} w_{c_2} w_{c_3} \cdot \begin{vmatrix} b & a & b \\ c_0 & c_0 & c_3 \end{vmatrix} \begin{vmatrix} b & a & b \\ c_1 & c_0 & c_0 \end{vmatrix} \\ & \cdot \begin{vmatrix} b & a & b \\ c_1 & c_1 & c_0 \end{vmatrix} \begin{vmatrix} b & a & b \\ c_2 & c_1 & c_1 \end{vmatrix} \\ & \cdot \begin{vmatrix} b & a & b \\ c_2 & c_2 & c_1 \end{vmatrix} \begin{vmatrix} b & a & b \\ c_3 & c_2 & c_2 \end{vmatrix} \\ & \cdot \begin{vmatrix} b & a & b \\ c_3 & c_3 & c_2 \end{vmatrix} \begin{vmatrix} b & a & b \\ c_0 & c_3 & c_3 \end{vmatrix}. \end{aligned}$$

Using Proposition 4.17 and a bit of reordering, we can rewrite the summation as:

$$\begin{aligned} TV_{r,s}(M_3, \mathcal{T}_3) = \sum_{(a,b,c_0,c_1,c_2,c_3) \in A_r(M_3,\mathcal{T}_3)} & w_a w_b w_{c_0} w_{c_1} w_{c_2} w_{c_3} \cdot \begin{vmatrix} a & b & b \\ c_0 & c_0 & c_3 \end{vmatrix} \begin{vmatrix} a & b & b \\ c_0 & c_0 & c_1 \end{vmatrix} \\ & \cdot \begin{vmatrix} a & b & b \\ c_1 & c_1 & c_0 \end{vmatrix} \begin{vmatrix} a & b & b \\ c_1 & c_1 & c_2 \end{vmatrix} \\ & \cdot \begin{vmatrix} a & b & b \\ c_2 & c_2 & c_1 \end{vmatrix} \begin{vmatrix} a & b & b \\ c_2 & c_2 & c_3 \end{vmatrix} \\ & \cdot \begin{vmatrix} a & b & b \\ c_3 & c_3 & c_2 \end{vmatrix} \begin{vmatrix} a & b & b \\ c_3 & c_3 & c_0 \end{vmatrix}. \end{aligned}$$

Chapter 5

Numerical evidences for the hyperbolic volume conjecture on M_2 and M_3

Let us recall the goal of this paper. We wish to numerically test the volume conjecture of [3] for M_2 and M_3, restated as follows:

Conjecture 5.1 (Conjecture 1.1, [3], Chen-Yang)**.** *Let M be a compact hyperbolic 3-manifold. Then for r running over all odd integers such that $r \geq 3$,*

$$\lim_{r\to\infty} \frac{2\pi}{r-2} \log\left(TV_{r,2}(M)\right) = Vol_H(M),$$

where $Vol_H(M)$ is the hyperbolic volume of M.

5.1 Numerical test on M_2

As constructed in Section 2.2.2, the manifold M_2 has the ordered ideal triangulation $\mathcal{T}_2$, shown in Figure 5.1, from which, in Section 6.1.3, we described the hyperbolic structure on M_2 and we calculated that

$$Vol_H(M_2) \approx 12.046092040094388.$$

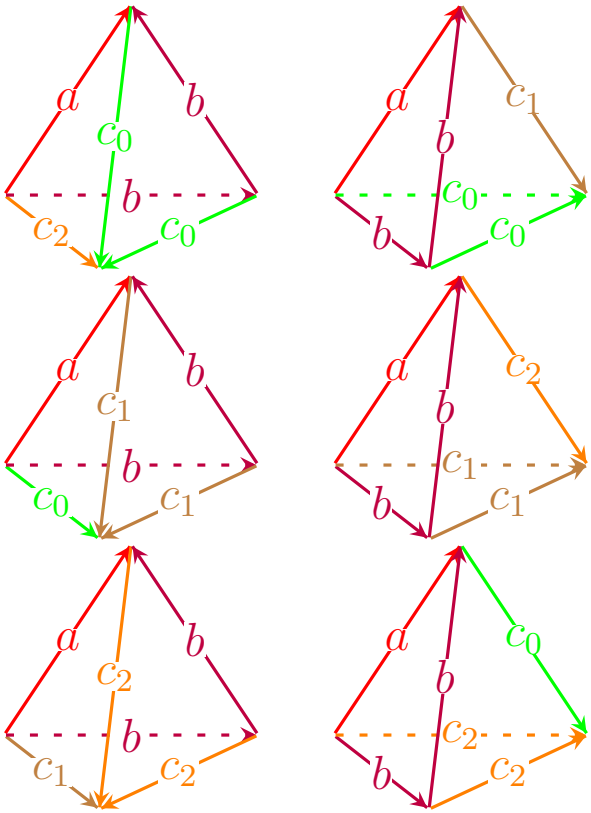

Figure 5.1: The ordered ideal triangulation of M_2

In Section 4.2.3, we determined that

$$TV_{r,2}(M_2,\mathcal{T}_2) = \sum_{(a,b,c_0,c_1,c_2)\in A_r(M_2,\mathcal{T}_2)} w_a w_b w_{c_0} w_{c_1} w_{c_2} \cdot \begin{vmatrix} a & b & b \\ c_0 & c_0 & c_2 \end{vmatrix} \begin{vmatrix} a & b & b \\ c_0 & c_0 & c_1 \end{vmatrix} \cdot \begin{vmatrix} a & b & b \\ c_1 & c_1 & c_0 \end{vmatrix} \begin{vmatrix} a & b & b \\ c_1 & c_1 & c_2 \end{vmatrix} \cdot \begin{vmatrix} a & b & b \\ c_2 & c_2 & c_1 \end{vmatrix} \begin{vmatrix} a & b & b \\ c_2 & c_2 & c_0 \end{vmatrix},$$

where $A_r(M_2,\mathcal{T}_2)$ consists of the 5-tuple (a,b,c_0,c_1,c_2) of elements of I_r such that they satisfy the conditions of Proposition 4.8. From this formula, we compute, using the code in Section 6.2, the table of values, shown in Figure 6.3, of the real part of

$$QV_{r,2}(M_2) := \frac{2\pi}{r-2}\log\left(TV_{r,2}(M_2,\mathcal{T}_2)\right)$$

for r running over odd integers such that $r \geq 3$. Note that for some r it happens that $TV_{r,2}(M_2,\mathcal{T}_2)$ is negative. Since we require the argument in the the logarithm function to be in $[0,2\pi]$, the imaginary part of $QV_{r,2}(M_2)$ is either 0 when $TV_{r,2}(M_2,\mathcal{T}_2)$ is positive or $\frac{2\pi^2}{r}$ when $TV_{r,2}(M_2,\mathcal{T}_2)$ is negative, which converges to 0 as $r \to \infty$. Therefore to test the convergence of $QV_{r,2}(M_2)$ we can forget about the imaginary parts and consider only the real parts. Figure 5.2 illustrates the asymptotic behaviour of $QV_{r,2}(M_2)$.

5.1.1 Interpretation for M_2

Numerical test 5.2. *The graph of $QV_{r,2}(M_2)$ (see Figure 5.2) shows a converging behaviour up to $r = 33$ and relative errors similar as in the literature.*

For example, we have that

$$\left|\frac{\mathcal{R}\left(QV_{31,2}(M_2)\right) - Vol_H(M_2)}{Vol_H(M_2)}\right| \approx \left|\frac{11.09819 - 12.04609}{12.04609}\right| \approx 7.869\%,$$

while in [3, Section 4] we have that

$$\left|\frac{QV_{31,2}(S^3 - K_{4_1}) - Vol_H\left(S^3 - K_{4_1}\right)}{Vol_H\left(S^3 - K_{4_1}\right)}\right| \approx \left|\frac{2.22824 - 2.02988}{2.02988}\right| \approx 9.772\%,$$

$$\left|\frac{QV_{31,2}(S^3 - K_{5_2}) - Vol_H\left(S^3 - K_{5_2}\right)}{Vol_H\left(S^3 - K_{5_2}\right)}\right| \approx \left|\frac{3.03657 - 2.82812}{2.82812}\right| \approx 7.368\%,$$

$$\left|\frac{QV_{31,2}(M_{min}) - Vol_H\left(M_{min}\right)}{Vol_H\left(M_{min}\right)}\right| \approx \left|\frac{5.4459 - 6.452}{6.452}\right| \approx 15.593\%.$$

Numerical test 5.3. *The graph of $QV_{r,2}(M_2)$ (see Figure 5.2) shows an unexpected and unusual increase in the values of $QV_{r,2}(M_2)$ after $r = 33$ such that it even surpasses the hyperbolic volume $Vol_H(M_2)$ at $r = 39$.*

Due to the increasing time required to compute $QV_{r,2}(M_2)$ as r grows, we were not able to go further in this thesis. We have several hypothesis on what might explain this behaviour:

- there might be an error in our code (see Section 6.2),
- there might be a computing error, due to an alternating sum that converges but where the term grows in absolute value, which causes the computer to stop the sum earlier than it should,
- the conjecture holds, but the convergence occurs with an oscillation around the hyperbolic volume, which we have not seen any example of in the literature,
- the conjecture is wrong for this 3-manifold, which would be really interesting.

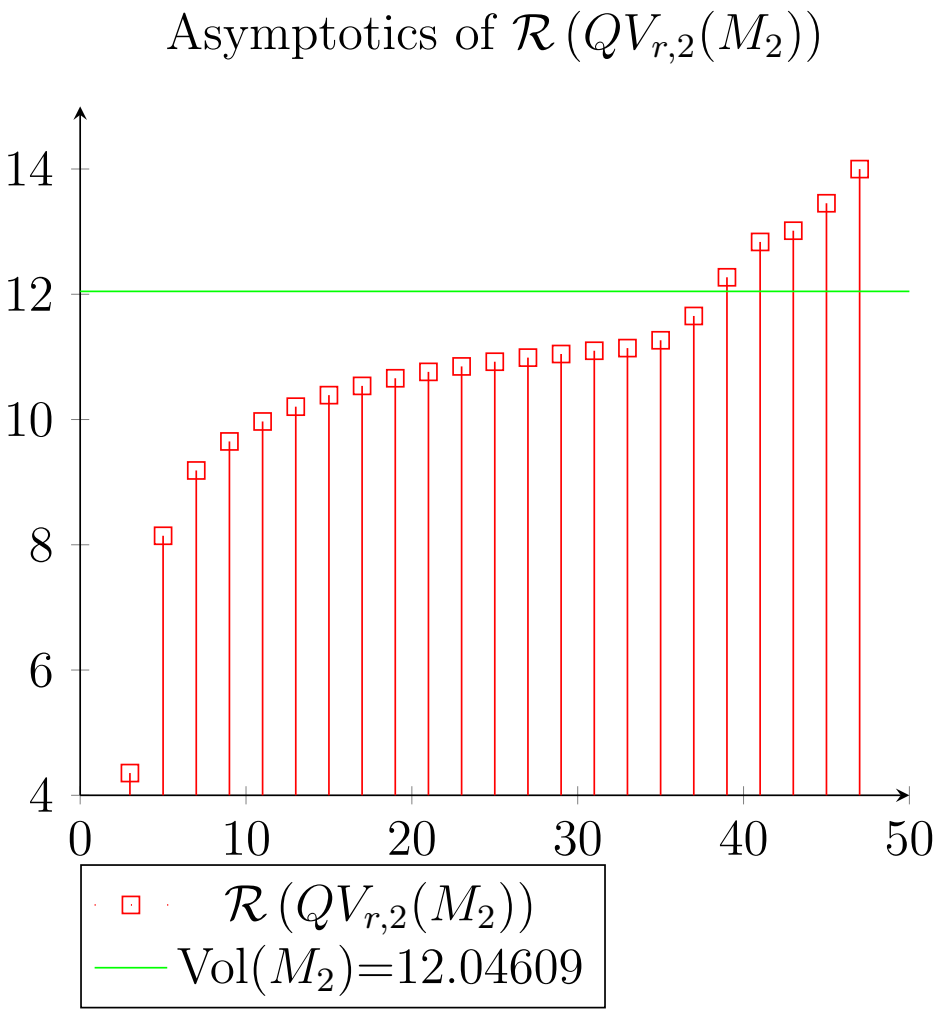

Figure 5.2: Graph of the values of $\mathcal{R}(QV_{r,2}(M_2))$ (shown in red) compared with the hyperbolic volume $\mathrm{Vol}(M_2)$ (shown in green).

5.2 Numerical test on M_3

As constructed in Section 2.2.1, the manifold M_3 has the ordered ideal triangulation $\mathcal{T}_3$, shown in Figure 5.2, from which, in Section 6.1.3, we described the hyperbolic structure on M_3 and we calculated that

$$Vol_H(M_3) \approx 18.03810545488482.$$

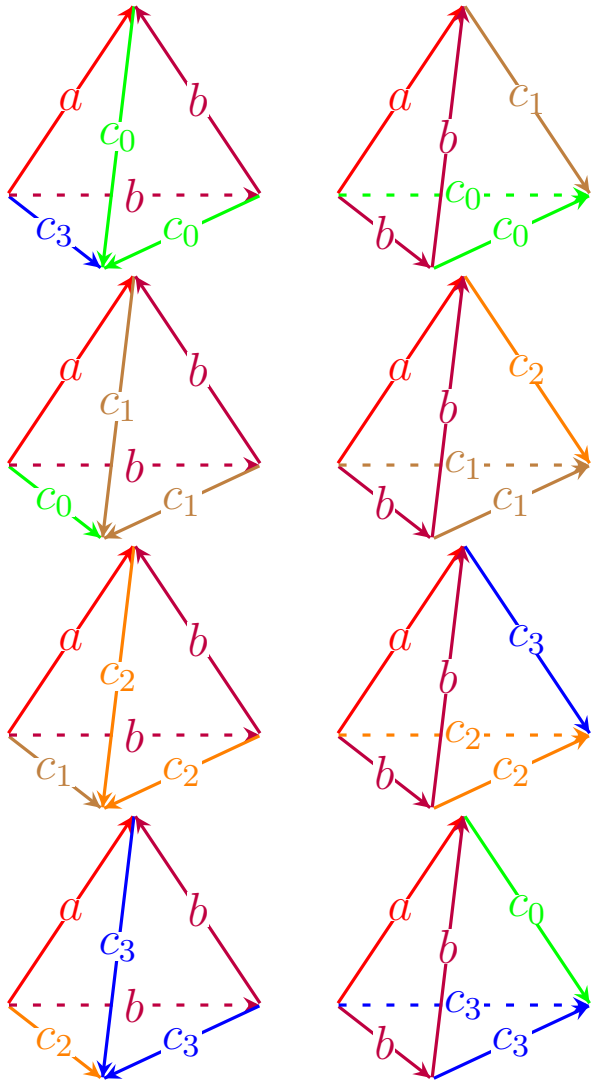

Figure 5.3: The ideal ordered triangulation of M_3

In Section 4.2.4, we determined that

$$TV_{r,2}(M_3,\mathcal{T}_3) = \sum_{(a,b,c_0,c_1,c_2,c_3)\in A_r(M_3,\mathcal{T}_3)} w_a w_b w_{c_0} w_{c_1} w_{c_2} \cdot \begin{vmatrix} a & b & b \\ c_0 & c_0 & c_3 \end{vmatrix} \begin{vmatrix} a & b & b \\ c_0 & c_0 & c_1 \end{vmatrix} \cdot \begin{vmatrix} a & b & b \\ c_1 & c_1 & c_0 \end{vmatrix} \begin{vmatrix} a & b & b \\ c_1 & c_1 & c_2 \end{vmatrix} \cdot \begin{vmatrix} a & b & b \\ c_2 & c_2 & c_1 \end{vmatrix} \begin{vmatrix} a & b & b \\ c_2 & c_2 & c_3 \end{vmatrix} \cdot \begin{vmatrix} a & b & b \\ c_3 & c_3 & c_2 \end{vmatrix} \begin{vmatrix} a & b & b \\ c_3 & c_3 & c_0 \end{vmatrix},$$

where $A_r(M_3,\mathcal{T}_3)$ consists of the 6-tuple (a,b,c_0,c_1,c_2,c_3) of elements of I_r such that

they satisfy the conditions of Proposition 4.8. From this formula, we compute, using the code in Section 6.2, the table of values, shown in Figure 6.4, of the real part of

$$QV_{r,2}(M_3) := \frac{2\pi}{r-2} \log\left(TV_{r,2}(M_3, \mathcal{T}_3)\right)$$

for r running over odd integers such that $r \geq 3$. Note that as $TV_{r,2}(M_2, \mathcal{T}_2)$, $TV_{r,2}(M_3, \mathcal{T}_3)$ might also be negative. For the same reasons as in Section 5.1, we can forget about the imaginary parts and consider only the real parts for the convergence. Figure 5.4 illustrates the asymptotic behaviour of $QV_{r,2}(M_3)$.

5.2.1 Interpretation for M_3

Numerical test 5.4. *The graph of $QV_{r,2}(M_3)$ (see Figure 5.4) shows a converging behaviour up to $r = 31$ and relative errors similar as in the literature.*

For example, we have that

$$\left|\frac{\mathcal{R}\left(QV_{31,2}(M_3)\right) - Vol_H(M_3)}{Vol_H(M_3)}\right| \approx \left|\frac{16.12064 - 18.0381}{18.0381}\right| \approx 12.531\%,$$

while in [3, Section 4] we have that

$$\left|\frac{QV_{31,2}(S^3 - K_{4_1}) - Vol_H\left(S^3 - K_{4_1}\right)}{Vol_H\left(S^3 - K_{4_1}\right)}\right| \approx \left|\frac{2.22824 - 2.02988}{2.02988}\right| \approx 9.772\%,$$

$$\left|\frac{QV_{31,2}(S^3 - K_{5_2}) - Vol_H\left(S^3 - K_{5_2}\right)}{Vol_H\left(S^3 - K_{5_2}\right)}\right| \approx \left|\frac{3.03657 - 2.82812}{2.82812}\right| \approx 7.368\%,$$

$$\left|\frac{QV_{31,2}(M_{min}) - Vol_H\left(M_{min}\right)}{Vol_H\left(M_{min}\right)}\right| \approx \left|\frac{5.4459 - 6.452}{6.452}\right| \approx 15.593\%.$$

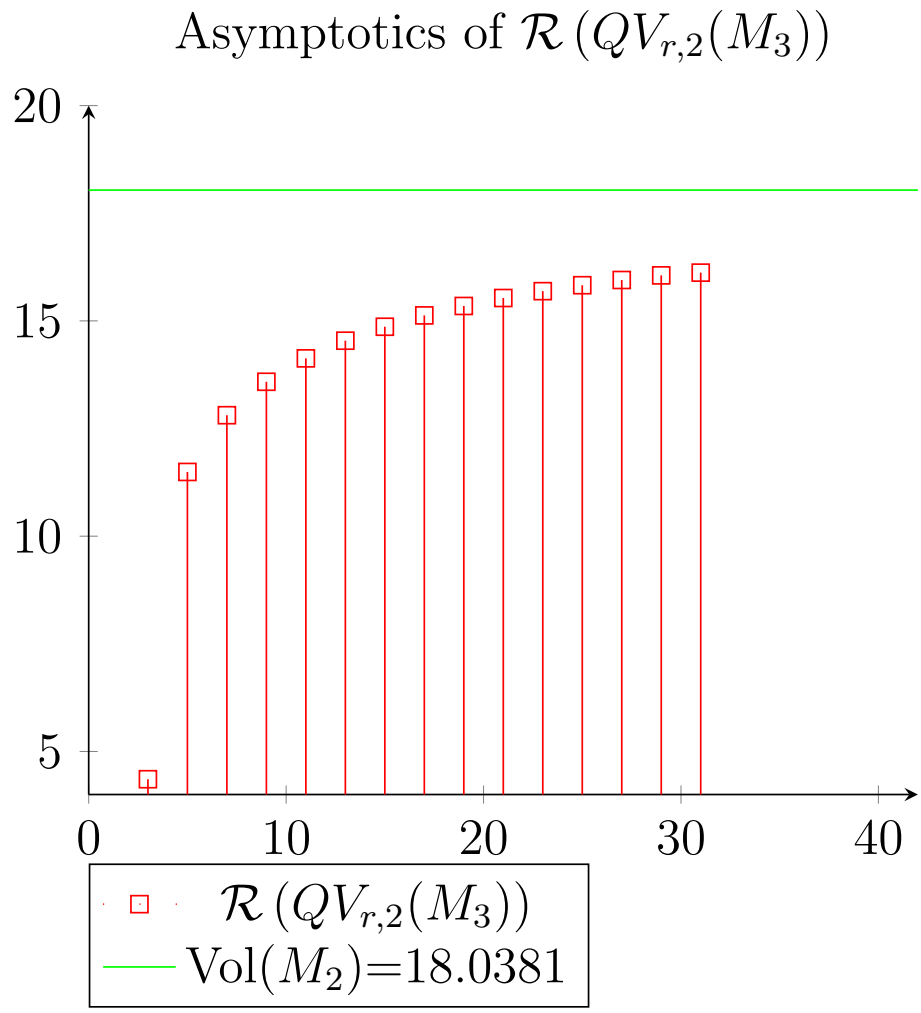

Figure 5.4: Graph of the values of $\mathcal{R}\left(QV_{r,2}(M_3)\right)$ (shown in red) compared with the hyperbolic volume Vol(M_3) (shown in green)

Chapter 6

Annotated code

The following codes have been written with SageMath, a free open-source mathematics software system using Python 3.

In this section, let us fix a pair $(r, s) \in \mathbb{N}^2$ such that $r \geq 3$ and $s \geq 1$.

Let $g \in \{2, 3, 4, ...\}$.

Notation. Let $\frac{\mathbb{N}}{2} = \{0, \frac{1}{2}, 1, ...\}$ denote the set of non-negative half integers.
Let $\frac{\mathbb{N}_{odd}}{2} = \{\frac{1}{2}, \frac{3}{2}, ...\}$ denote the set of non-negative half-odd-integers.
Let I_r denote the subset $\left\{0, \frac{1}{2}, 1, ..., \frac{r-2}{2}\right\}$ of $\frac{\mathbb{N}}{2}$.

6.1 Computing the hyperbolic volume of M_g

In this section, we will first construct a function which computes the volume of a tetrahedron from its dihedral angles, via the volume formula for generalized hyperbolic tetrahedra proved by Ushijima in [13, Theorem 1.1]. We will apply this formula for the tetrahedra in the triangulation $(M_2, \mathcal{T}_2)$ (defined in Section 2.2.1) and we will obtain a numerical approximation of the hyperbolic volume of M_2. Lastly, we will generalise this process in order to have a function giving us the hyperbolic volume of M_g for a given $g \geq 2$.

6.1.1 The volume formula for hyperbolic tetrahedra

We first import the *NumPy* package which is an easy to use, performant and open source package in Python. This package notably contains the function **pi** giving an approximate value of π that we will use later on. Functions imported from this package will be written in the code with the prefix **np.**, which means we access the function inside the package *NumPy*.

```
1 import numpy as np
```

Listing 6.1: Importing NumPy

Let $T = T(A, B, C, D, E, F)$ be a generalized tetrahedron in the three dimensional hyperbolic space $\mathbb{H}^3$ whose dihedral angles are $A, B, C, D, E, F \in [0, \pi]$ (see Definitions 3.8 and 3.5). The configuration of the dihedral angles is as in Figure 6.1.

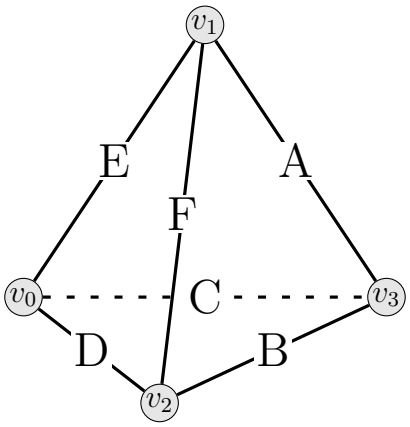

Figure 6.1: The configuration of dihedral angles on T

Let G be the Gram matrix of T defined as follows:

$$G = \begin{pmatrix} 1 & -\cos A & -\cos B & -\cos F \\ -\cos A & 1 & -\cos C & -\cos E \\ -\cos B & -\cos C & 1 & -\cos D \\ -\cos F & -\cos E & -\cos D & 1 \end{pmatrix}.$$

It should be noted that this definition of the Gram matrix is slightly different from the ordinary one (see [13, Theorem 3.2]). By [13, Theorem 3.2], G has three positive and one negative eigenvalues. Thus its determinant $\det(G)$ is always negative.

The function **Gramdet(A,B,C,D,E,F)** computes the determinant of the previous Gram matrix for given values of $A, B, C, D, E, F \in [0, \pi]$.

```
import numpy as np

def Gramdet(A,B,C,D,E,F):
    G = matrix([  [1,-cos(A),-cos(B),-cos(F)],
            [-cos(A),1,-cos(C),-cos(E)],
            [-cos(B),-cos(C),1,-cos(D)],
            [-cos(F),-cos(E),-cos(D),1]])
    res = G.determinant()
    return res
```

Listing 6.2: The determinant of the Gram matrix of T

Let $Li_2(z)$ be the dilogarithm function defined in [13, Introduction] by the analytic continuation of the following integral:

$$Li_2(x) := -\int_0^x \frac{\log(1-t)}{t}\mathrm{d}t \quad \text{for } x \in \mathbb{R}_{>0}.$$

Let I be the principal square root of -1 , $a := \exp(I \cdot A)$, $b := \exp(I \cdot B)$, ..., $F := \exp(I \cdot F)$ and let $U(z, T)$ be the complex valued function defined as follows:

$$\begin{aligned} U(z,T) := \frac{1}{2}(&Li_2(z) + Li_2(abdez) + Li_2(acdfz) + Li_2(bcefz) \\ &- Li_2(-abcz) - Li_2(-aefz) - Li_2(-bdfz) - Li_2(-cdez)). \end{aligned}$$

The **U(z,A,B,C,D,E,F)** function computes $U(z, T)$ for a given complex number z and the dihedral angles A, B, C, D, E and F of a given generalized tetrahedron T. We use the **dilog(z)** function for z a complex number to compute $Li_2(z)$.

```
def U(z,A,B,C,D,E,F):
    a = exp(I*A)
    b = exp(I*B)
    c = exp(I*C)
    d = exp(I*D)
    e = exp(I*E)
    f = exp(I*F)

    z1 = a*b*d*e*z
    z2 = a*c*d*f*z
    z3 = b*c*e*f*z
    z4 = -a*b*c*z
    z5 = -a*e*f*z
    z6 = -b*d*f*z
    z7 = -c*d*e*z

```

```
    res = 1/2*(dilog(z)+dilog(z1)+dilog(z2)+dilog(z3)-dilog(z4)-dilog(
    z5)-dilog(z6)-dilog(z7))
    return res
```

Listing 6.3: The complex valued fonction $U(z,T)$

We denote by z_1 and z_2 the two complex numbers defined as follows:

$$z_1 := -2\frac{\sin A \sin D + \sin B \sin E + \sin C \sin F - \sqrt{\det G}}{ad+be+cf+abf+ace+bcd+def+abcdef},$$
$$z_2 := -2\frac{\sin A \sin D + \sin B \sin E + \sin C \sin F + \sqrt{\det G}}{ad+be+cf+abf+ace+bcd+def+abcdef},$$

where $\sqrt{\det G} \in I\mathbb{R}_{>0}$ is the principal square root of $\det G$.

We recall the following theorem from Section 3.2.

Theorem 6.1 (Ushijima, Theorem 1.1,[13])**.** *The hyperbolic volume Vol(T) of a generalized tetrahedron $T = T(A,B,C,D,E,F)$ is given as follows:*

$$Vol(T) = \frac{1}{2}\mathcal{I}(U(z_1,T) - U(z_2,T))$$

where $\mathcal{I}$ means the imaginary part.

The **TetVolum(A,B,C,D,E,F)** function uses the previous formula to compute the hyperbolic volume of a tetrahedron given its dihedral angles A, B, C, D, E and F.

```
def TetVolum(A,B,C,D,E,F):
    a = exp(I*A)
    b = exp(I*B)
    c = exp(I*C)
    d = exp(I*D)
    e = exp(I*E)
    f = exp(I*F)

    det = Gramdet(A,B,C,D,E,F)

    z = -2*((sin(A)*sin(D)+sin(B)*sin(E)+sin(C)*sin(F)-sqrt(det))/(a*d+
    b*e+c*f+a*b*f+a*c*e+b*c*d+d*e*f+a*b*c*d*e*f))

    zbis = -2*((sin(A)*sin(D)+sin(B)*sin(E)+sin(C)*sin(F)+sqrt(det))/(a
    *d+b*e+c*f+a*b*f+a*c*e+b*c*d+d*e*f+a*b*c*d*e*f))

    res = imag((U(z,A,B,C,D,E,F)-U(zbis,A,B,C,D,E,F))/2)

    return res
```

Listing 6.4: The hyperbolic volume of T

6.1.2 Applying the volume formula on tetrahedra of $\mathcal{T}_2$

In [5, Section 2], Frigerio provides the geometric angle structure on the tetrahedra of the ideal triangulation $\mathcal{T}_2$ that corresponds to the unique complete hyperbolic structure on the manifold M_2. Setting $\alpha_2 = \frac{\pi}{6}$, $\beta_2 = 2\alpha_2$, $\gamma_2 = \arccos((2\cos\alpha_2)^{-1})$ and $\delta_2 = \pi - 2\gamma_2$, Frigerio's angle structure is as in Figure 3.3.

In the following part of the code, we compute the hyperbolic volume of M_2, as the sum of the volumes of the six generalized hyperbolic tetrahedra of Figure 3.3. Three of them have dihedral angles $(A, B, C, D, E, F) = (\alpha_2, \delta_2, \alpha_2, \gamma_2, \beta_2, \gamma_2)$ and the three others have dihedral angles $(A, B, C, D, E, F) = (\gamma_2, \delta_2, \gamma_2, \alpha_2, \beta_2, \alpha_2)$.

```
Alpha2=np.pi/6
Beta2=2*Alpha2
Gamma2=arccos(1/(2*cos(Alpha2)))
Delta2=np.pi - 2*Gamma2

print(3*TetVolum(Alpha2,Delta2,Alpha2,Gamma2,Beta2,Gamma2)+3*TetVolum(
    Gamma2,Delta2,Gamma2,Alpha2,Beta2,Alpha2))
```

Listing 6.5: Computing the hyperbolic volume of M_2 (1)

Note that the volume formula is symmetric under the permutation of two dihedral angles (see [13, Section 5]), thus all the tetrahedra in $\mathcal{T}_2$ have the same hyperbolic volume (it can be seen by permuting the two α_2 with the two γ_2). We can thus multiply this hyperbolic volume by six (the number of tetrahedra) to obtain the hyperbolic volume of M_2.

```
print(6*TetVolum(Gamma2,Delta2,Gamma2,Alpha2,Beta2,Alpha2))
```

Listing 6.6: Computing the hyperbolic volume of M_2 (2)

Both previous computations yield the following hyperbolic volume.

```
12.046092040094388
```

Listing 6.7: The hyperbolic volume of M_2

This value is the same as mentioned in [6, Example 3], which gives confidence in our code.

6.1.3 Applying the volume formula on tetrahedra of $\mathcal{T}_g$

In [5, Section 2], Frigerio provides the unique angle structure on the tetrahedra of the ideal triangulation $\mathcal{T}_g$ that corresponds to the unique complete hyperbolic structure on the manifold M_g. Setting $\alpha_g = \frac{\pi}{2g+2}$, $\beta_g = 2\alpha_g$, $\gamma_g = \arccos((2\cos\alpha_g)^{-1})$ and $\delta_g = \pi - 2\gamma_g$, Frigerio's angle structure of the triangulation $\mathcal{T}_g$ is similar as the one for $\mathcal{T}_2$ in Figure 3.3. However, instead of having three tetrahedra sharing an angle structure and the three other tetrahedra sharing another, there are $g+1$ tetrahedra sharing an angle structure and the $g+1$ other tetrahedra sharing another. You can see those two different angle structures in Figure 6.2.

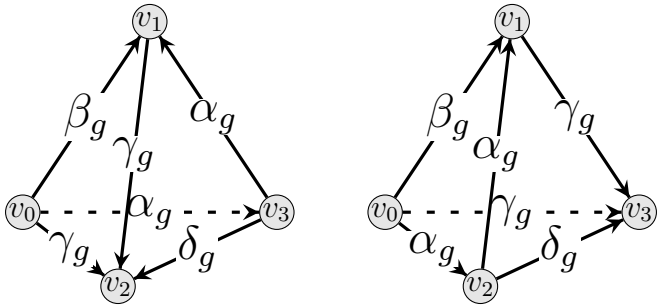

Figure 6.2: Frigerio's angle structure on $\mathcal{T}_g$

We can thus generalize the previous code to create the **HyperbolicVolume(g)** function which computes the hyperbolic volume of M_g given $g \in \{2, 3, 4, ...\}$, by computing the hyperbolic volume of one tetrahedron and multiplying it by $2g+2$, the number of tetrahedra in the triangulation. As for $\mathcal{T}_2$, (by permuting the two α_g with the two γ_g in the hyperbolic volume formula) we have that each tetrahedron has the same hyperbolic volume. We have shown the result for this function for some values of g in Figure 1.1.

```
def HyperbolicVolume(g):

  Alphag=np.pi/(2*g+2)
  Betag=2*Alphag
  Gammag=arccos(1/(2*cos(Alphag)))
  Deltag=np.pi - 2*Gammag

  res=(2*g+2)*TetVolum(Gammag,Deltag,Gammag,Alphag,Betag,Alphag)

  return res
```

Listing 6.8: The hyperbolic volume of M_g for a given g

6.2 Computing the Turaev-Viro invariants $TV_{r,s}(M_g, \mathcal{T}_g)$

In this section, we will construct several functions in order to compute the Turaev-Viro invariants $TV_{r,s}(M_2, \mathcal{T}_2)$ and $TV_{r,s}(M_3, \mathcal{T}_3)$ given $(r, s) \in \mathbb{N}^2$ such that $r \geq 3$ and $s \geq 1$. These functions can easily be extended to compute the other Turaev-Viro invariants $TV_{r,s}(M_g, \mathcal{T}_g)$ for $g \geq 4$. We will refer to definitions of Section 4.2 as needed.

We first import the *NumPy* package as in Appendix 6.1.1. We also import the *cmath* package which gives us mathematical functions for complex numbers, such as square roots for negative numbers. Functions imported from *cmath* will be written with the prefix **cm.**.

```
import numpy as np
import cmath as cm
```

Listing 6.9: Importing NumPy and cmath

The function **quantum_number(r,s,n)** returns the quantum number $[n]$ given r, s and $n \in \mathbb{N}$ (see Definition 4.9).

```
def quantum_number(r,s,n):

    res=sin(s*n*(np.pi)/r)/sin(s*(np.pi)/r)

    return res
```

Listing 6.10: Quantum number

The function **quantum_factorial(r,s,n)** returns the factorial of a quantum number $[n]!$ given r, s and $n \in \mathbb{N}$ (see Definition 4.11). If $n = 0$, then the factorial $[0]!$ is defined to be 1. If $n \geq 1$, then the factorial is computed via the **prod()** function which returns the product of all elements in a given list. The list in question is created by using the **range()** function, which gives an integer list of numbers ranging from the first term to the penultimate term (here $\{1, 2, 3, ..., n\}$), and the function **quantum_number(r,s,i)** for fixed r and s and $i \in \{1, 2, 3, ..., n\}$.

```
def quantum_factorial(r,s,n):

    if n == 0:
        return 1

    return prod([quantum_number(r,s,i) for i in range(1, n+1)])
```

Listing 6.11: Quantum factorial

The function **q_big_delta_coeff(i,j,k,r,s)** returns the coefficients

$$\Delta(i,j,k) := \sqrt{\frac{[i+j-k]![i-j+k]![-i+j+k]!}{[i+j+k+1]!}}$$

given r, s and (i,j,k) an admissible triple of elements of I_r (see Definition 4.13). Admissibility conditions (see Definition 4.1) ensure that $i+j-k$, $i+k-j$, $j+k-i$ and $i+j+k+1$ are in $\mathbb{N}$ but since the values of i, j and k can be half integers, the values $i+k-j$, $j+k-i$ and $i+j+k+1$ are stored as rational type variable. To ensure that the function **quantum_factorial()** works, we have to change their type from rational to integers using the $int()$ function.

Since **quantum_number()** and thus **quantum_factorial()** can return negative values, then the term we take the square root of might be negative. We thus need to use the function **cm.sqrt()**, i.e the complex square root from the *cmath* package.

```
def q_big_delta_coeff(i,j,k,r,s):

    argsqrt = (quantum_factorial(r,s,int(i + j - k)) * \
               quantum_factorial(r,s,int(i + k - j)) * \
               quantum_factorial(r,s,int(j + k - i))) / \
               quantum_factorial(r,s,int(i + j + k + 1))

    res = cm.sqrt(argsqrt)

    return res
```

Listing 6.12: Δ coefficients

The function **q_symbol(i, j, k, l, m, n, r, s)** returns the quantum $6j$-symbols

$$\begin{vmatrix} i & j & k \\ l & m & n \end{vmatrix} := \sqrt{-1}^{-2(i+j+k+l+m+n)} \Delta(i,j,k)\Delta(j,l,n)\Delta(i,m,n)\Delta(k,l,m)$$
$$\cdot \sum_{z=\max\{T_1,T_2,T_3,T_4\}}^{\min\{Q_1,Q_2,Q_3\}} \frac{(-1)^z[z+1]!}{[z-T_1]![z-T_2]![z-T_3]![z-T_4]![Q_1-z]![Q_2-z]![Q_3-z]!}$$

given r, s and (i,j,k,l,m,n) a 6-tuple of elements of I_r such that (i,j,k), (j,l,n), (i,m,n) and (k,l,m) are admissible (see Definition 4.15). First, we compute the term

$$\text{prefac} = \Delta(i,j,k)\Delta(j,l,n)\Delta(i,m,n)\Delta(k,l,m)$$

by using the function **q_big_delta_coeff()**. We then determine the upper bound z_{max} and lower bound z_{min} of the sum in Definition 4.15. We use the **range()** function to create a loop that will goes each integer value between z_{min} included and $z_{max}+1$

excluded. Before the loop, we create a variable *sumres* equal to 0. For each value of z, we compute the term

$$\frac{(-1)^z[z+1]!}{[z-T_1]![z-T_2]![z-T_3]![z-T_4]![Q_1-z]![Q_2-z]![Q_3-z]!}$$

using the function **quantum_factorial()** and add it to the *sumres* variable. When the loop ends, the *sumres* variable is equal to

$$\sum_{z=\max\{T_1,T_2,T_3,T_4\}}^{\min\{Q_1,Q_2,Q_3\}} \frac{(-1)^z[z+1]!}{[z-T_1]![z-T_2]![z-T_3]![z-T_4]![Q_1-z]![Q_2-z]![Q_3-z]!}.$$

Lastly, we take the product of the *prefac* and *sumres* variables with $\sqrt{-1}^{-2(i+j+k+l+m+n)}$, which gives the desired result for our function.

```
def q_symbol(i, j, k, l, m, n, r, s):

    prefac = q_big_delta_coeff(i, j, k, r, s) * \
             q_big_delta_coeff(j, l, n, r, s) * \
             q_big_delta_coeff(i, m, n, r, s) * \
             q_big_delta_coeff(k, l, m, r, s)


    zmin = max(i + j + k, j + l + n, i + m + n, k + l + m)
    zmax = min(i + j + l + m, i + k + l + n, j + k + m + n)

    sumres = 0
    for z in range(int(zmin), int(zmax) + 1):
        den = quantum_factorial(r,s,int(z - (i + j + k))) * \
              quantum_factorial(r,s,int(z - (j + l + n))) * \
              quantum_factorial(r,s,int(z - (i + m + n))) * \
              quantum_factorial(r,s,int(z - (k + l + m))) * \
              quantum_factorial(r,s,int(i + j + l + m - z)) * \
              quantum_factorial(r,s,int(i + k + l + n - z)) * \
              quantum_factorial(r,s,int(j + k + m + n - z))

        sumres = sumres + (((-1) ** z) * quantum_factorial(r,s,int(z +
    1))) / den

    res = prefac * sumres * sqrt(-1)**(int(2*(i+j+k+l+m+n)))
    return res
```

Listing 6.13: Quantum *6j*-symbols

The function **edge(a,r,s)** computes the edge term $w_a := (-1)^{2a}[2a+1]$ (see Definition 4.20) given r, s and $a \in I_r$ using the function **quantum_number()**.

```
def edge(a,r,s) :

    res = ((-1)**(2*a))*quantum_number(r,s,int(2*a+1))

    return res
```

Listing 6.14: Edge term

The function **term(a,b,c,g,r,s)** computes a term of the sum in the Definition 4.22 applied to $(M_g, \mathcal{T}_g)$ given $a \in I_r$, $b \in I_r$, $c = (c_0, c_1, c_2, ..., c_g) \in I_r^{g+1}$, $g \in \{2, 3, 4, ...\}$, r and s such that they satisfy the conditions in Proposition 4.8 (see Section 4.2.3 for the case of $g = 2$). We start by taking the product $res = w_a w_b$ of the terms of the edges labelled by a and b, using the function **edge()**. Then we create a loop using the function **range()**. This loop starts at $i = 0$ by multiplying together the variable res, the quantum $6j$-symbols $\begin{vmatrix} a & b & b \\ c_0 & c_0 & c_g \end{vmatrix}$, $\begin{vmatrix} a & b & b \\ c_0 & c_0 & c_1 \end{vmatrix}$ and the term of the edge labelled by c_0, w_{c_0}. The quantum $6j$-symbols are determined by the function **q_symbol()**. The loop continues and, at each iteration $i \in \{1, 2, ..., g-1\}$, we multiply the res variable with the quantum $6j$-symbols $\begin{vmatrix} a & b & b \\ c_i & c_i & c_{i-1} \end{vmatrix}$, $\begin{vmatrix} a & b & b \\ c_i & c_i & c_{i+1} \end{vmatrix}$ and the edge term w_{c_i}. The loop ends at $i = g$ where the res variable is multiplied by the quantum $6j$-symbols $\begin{vmatrix} a & b & b \\ c_g & c_g & c_{g-1} \end{vmatrix}$, $\begin{vmatrix} a & b & b \\ c_g & c_g & c_0 \end{vmatrix}$ and the edge term w_{c_g}.

```
def term(a,b,c,g,r,s):

    res=edge(a, r, s)*edge(b, r, s)

    for i in range(g+1):
        if i==0:
            res = res * edge(c[i], r, s) * \
                  q_symbol(a, b, b, c[i], c[i], c[g], r, s) * \
                  q_symbol(a, b, b, c[i], c[i], c[i+1], r, s)
        elif i==g:
            res = res * edge(c[i], r, s) * \
                  q_symbol(a, b, b, c[i], c[i], c[i-1], r, s) * \
                  q_symbol(a, b, b, c[i], c[i], c[0], r, s)
        else:
            res = res * edge(c[i], r, s) * \
                  q_symbol(a, b, b, c[i], c[i], c[i-1], r, s) * \
                  q_symbol(a, b, b, c[i], c[i], c[i+1], r, s)

    return res
```

Listing 6.15: One term of the sum in $TV_{r,s}(M_g, \mathcal{T}_g)$ for a given admissible colouring

The function **turaevvirog2(r,s)** computes $TV_{r,s}(M_2, \mathcal{T}_2)$, while the function **turaevvirog3(r,s)** computes $TV_{r,s}(M_3, \mathcal{T}_3)$ given r and s (see Sections 4.2.3 and 4.2.4). These two functions consists in listing all the admissible colourings of Proposition 4.8 and computing the associated term contributing to the sum in $TV_{r,s}(M_g, \mathcal{T}_g)$ via the **term()** function for $g \in \{2, 3\}$. We will follow the numeration of the conditions in Proposition 4.8 to ensure we go trough each of them.

Let $a, b, c_0, ..., c_g \in I_r$.

For the colouring to be admissible, a has to satisfy the following condition:

(1) $a \in \mathbb{N}$.

The first loop is over the label a which covers all integers from 0 to $\frac{r-2}{2}$. We will refer to it as the a loop. The **floor()** function ensures that the a loop ends at $\lfloor \frac{r-2}{2} \rfloor$.

For a fixed a and an admissible colouring, b has to satisfy the two following conditions:

(2) $b \in \mathbb{N}$,

(4) $\frac{a}{2} \leq b \leq \frac{r-2-a}{2}$.

We create thus, inside the a loop, a second loop over the label b, the b loop, which covers all integers from $\frac{a}{2}$ to $\frac{r-2-a}{2}$. The **floor()** function and the $+1$ ensure that the b loop ends at $\lfloor \frac{r-2-a}{2} \rfloor$ while the **ceil()** function ensures that the b loop starts at $\lceil \frac{a}{2} \rceil$.

For an admissible colouring, the labels c_i (for $i \in \{0, 1, 2, ..., g\}$) have to satisfy the following condition:

(3) either $(\forall i \in \{0, 1, 2, ..., g\},\ c_i \in \mathbb{N})$ or $(\forall i \in \{0, 1, 2, ..., g\},\ c_i \in \frac{\mathbb{N}_{odd}}{2})$.

We denote those two categories as integer states and half-integer states. Thus, we create two different loops inside the b loop, one for the integer states and the other one for the half-integer states.

Let us start with the integer states, i.e $(\forall i \in \{0, 1, 2, ..., g\},\ c_i \in \mathbb{N})$. For a fixed b and an admissible colouring, the label c_0 has to satisfy the following condition:

(6a) $\frac{b}{2} \leq c_0 \leq \frac{r-2-b}{2}$.

We create thus, inside the b loop, a loop over the label c_0, the c_0 loop, which covers all integers from $\lceil \frac{b}{2} \rceil$ to $\lfloor \frac{r-2-b}{2} \rfloor$.

For $i \in \{0, ..., g-1\}$, for fixed a, b, c_i and an admissible colouring, the label c_{i+1} has to satisfy the following conditions:

(5a) $\frac{b}{2} \leq c_{i+1} \leq \frac{r-2-b}{2}$,

(5b) $a - c_i \leq c_{i+1} \leq r - 2 - a - c_i$,

(5c-d) $c_i - \min(a, b) \leq c_{i+1} \leq c_i + \min(a, b)$.

For all $i \in \{0, ..., g-1\}$, we create in the loop c_i two variables m_{i+1} (the maximum of the three lower bounds on c_{i+1}) and M_{i+1} (the minimum of the three upper bounds on c_{i+1}). We create thus, inside the c_i loop, a loop over the label c_{i+1}, the c_{i+1} loop, which ranges to all integers from $\lceil m_{i+1} \rceil$ to $\lfloor M_{i+1} \rfloor$. For fixed a, b, c_0, c_1, ... and c_g, for the colouring to be admissible, the following conditions have also to be satisfied:

(6b) $a - c_g \leq c_0 \leq r - 2 - a - c_g$,

(6c-d) $c_g - \min(a, b) \leq c_0 \leq c_g + \min(a, b)$.

We add thus an **if** loop that checks those two conditions. If those are satisfied, we compute the term associated to the colouring $(a, b, c_0, c_1, ..., c_g)$ via the function **term()**.

Once we have covered all the integer states, we create inside the b loop, a second loop over the label c_0, the c_0 *bis* loop, which covers all half-integers from $\lfloor \frac{b}{2} \rfloor + \frac{1}{2}$ to $\lceil \frac{r-2-b}{2} \rceil - \frac{1}{2}$. The function **np.arange()** allows us to start and end loops at non-integer values and specify the step of the loop to be 1. The rest of the c_0 *bis* loop is constructed in the same way as for the c_0 loop, but the nested loops are over half-integers instead of integers.

As proved in Proposition 4.8, the previously constructed loops go over all admissible states, thus we get an approximate value of $TV_{r,s}(M_g, \mathcal{T}_g)$ for $g \in \{2, 3\}$. In the same way, one could construct a function which computes $TV_{r,s}(M_g, \mathcal{T}_g)$ for $g \geq 4$.

We have constructed only the $g = 2$ and $g = 3$ cases for two reasons. Firstly, because we did not create a general function for a given g and thus we had to create by hand each function. We had to limit ourselves. Secondly, with greater g comes more loops which tends to increase the time needed for the function to compute. This is why we could not compute further than $r = 31$ for the case $g = 3$ in Figure 5.4, while we went up to $r = 41$ for the case $g = 2$ in Figure 5.2.

```
def turaevvirog2(r,s):
    res= 0
    for a in range(floor((r-2)/2)+1):
        for b in range(ceil(a/2),floor((r-2-a)/2)+1):
            m=min(a,b)
            for c0 in range(ceil(b/2),floor((r-2-b)/2)+1):
                m1=max(c0-m,a-c0,b/2)
                M1=min(c0+m,r-2-a-c0,(r-2-b)/2)
                for c1 in range(ceil(m1),floor(M1)+1):
                    m2=max(c1-m,a-c1,b/2)
                    M2=min(c1+m,r-2-a-c1,(r-2-b)/2)
                    for c2 in range(ceil(m2),floor(M2)+1):
                        if (-m<=c2-c0<=m) and (a<=c2+c0<=r-2-a):
                            c=[c0,c1,c2]
                            res=res+term(a,b,c,2,r,s)

            for c0 in np.arange(floor(b/2)+1/2,ceil((r-2-b)/2),1):
                m1=max(c0-m,a-c0,b/2)
                M1=min(c0+m,r-2-a-c0,(r-2-b)/2)
                for c1 in np.arange(floor(m1)+1/2,ceil(M1),1):
                    m2=max(c1-m,a-c1,b/2)
                    M2=min(c1+m,r-2-a-c1,(r-2-b)/2)
                    for c2 in np.arange(floor(m2)+1/2,ceil(M2),1):
                        if (-m<=c2-c0<=m) and (a<=c2+c0<=r-2-a):
                            c=[c0,c1,c2]
                            res=res+term(a,b,c,2,r,s)
    return res
```

Listing 6.16: $TV_{r,s}(M_2, \mathcal{T}_2)$

```
def turaevvirog3(r,s):
    res= 0
    for a in range(floor((r-2)/2)+1):
        for b in np.arange(ceil(a/2),floor((r-2-a)/2)+1,1):
            m=min(a,b)
            for c0 in np.arange(ceil(b/2),floor((r-2-b)/2)+1,1):
                m1=max(c0-m,a-c0,b/2)
                M1=min(c0+m,r-2-a-c0,(r-2-b)/2)
                for c1 in np.arange(ceil(m1),floor(M1)+1,1):
                    m2=max(c1-m,a-c1,b/2)
                    M2=min(c1+m,r-2-a-c1,(r-2-b)/2)
                    for c2 in np.arange(ceil(m2),floor(M2)+1,1):
                        m3=max(c2-m,a-c2,b/2)
                        M3=min(c2+m,r-2-a-c2,(r-2-b)/2)
                        for c3 in np.arange(ceil(m3),floor(M3)+1,1):
                            if (-m<=c3-c0<=m) and (a<=c3+c0<=r-2-a):
                                c=[c0,c1,c2,c3]
                                res=res+term(a,b,c,3,r,s)

            for c0 in np.arange(floor(b/2)+1/2,ceil((r-2-b)/2),1):
                m1=max(c0-m,a-c0,b/2)
                M1=min(c0+m,r-2-a-c0,(r-2-b)/2)
                for c1 in np.arange(floor(m1)+1/2,ceil(M1),1):
                    m2=max(c1-m,a-c1,b/2)
                    M2=min(c1+m,r-2-a-c1,(r-2-b)/2)
                    for c2 in np.arange(floor(m2)+1/2,ceil(M2),1):
                        m3=max(c2-m,a-c2,b/2)
                        M3=min(c2+m,r-2-a-c2,(r-2-b)/2)
                        for c3 in np.arange(floor(m3)+1/2,ceil(M3),1):
                            if (-m<=c3-c0<=m) and (a<=c3+c0<=r-2-a):
                                c=[c0,c1,c2,c3]
                                res=res+term(a,b,c,3,r,s)
    return res
```

Listing 6.17: $TV_{r,s}(M_3, \mathcal{T}_3)$

6.3 Asymptotic behaviour of $QV_{r,2}(M_2)$ and $QV_{r,2}(M_3)$

The function **quantumvirog2(r,s)** computes $QV_{r,s}(M_2) = \frac{s\pi}{r-2} \log\left(TV_{r,s}(M_2, \mathcal{T}_2)\right)$ given $(r, s) \in \mathbb{N}^2$ such that $r \geq 3$ and $s \geq 1$.

```
def quantumvirog2(r,s):
    res=(s*(np.pi)/(r-2))*log(turaevvirog2(r,s))
    return res
```

Listing 6.18: $QV_{r,s}(M_2, \mathcal{T}_2)$

The function **quantumvirog3(r,s)** computes $QV_{r,s}(M_3) = \frac{s\pi}{r-2} \log\left(TV_{r,s}(M_3, \mathcal{T}_3)\right)$ $(r, s) \in \mathbb{N}^2$ such that $r \geq 3$ and $s \geq 1$.

```
def quantumvirog3(r,s):
    res=(s*(np.pi)/(r-2))*log(turaevvirog3(r,s))
    return res
```

Listing 6.19: $QV_{r,s}(M_3, \mathcal{T}_3)$

We set $s = 2$ in order to numerically compute $QV_{r,2}(M_2)$ and $QV_{r,2}(M_3)$ and take only their real part (the reason for taking the real part is explained in Section 5.1).

We use the function **quantumvirog2(r,s)** for $s = 2$ and increasing values of r, and we obtain the table of values of $\mathcal{R}\left(QV_{r,2}(M_2)\right)$ shown in Figure 6.3 and in Figure 5.2.

r	3	5	7	9	11	13
$\mathcal{R}\left(QV_{r,2}(M_2)\right)$	4.35517	8.14385	9.18650	9.65004	9.96879	10.20513

r	15	17	19	21	23	25
$\mathcal{R}\left(QV_{r,2}(M_2)\right)$	10.38914	10.53704	10.65879	10.76091	10.84790	10.92297

r	27	29	31	33	35	37
$\mathcal{R}\left(QV_{r,2}(M_2)\right)$	10.98846	11.04617	11.09819	11.14052	11.26531	11.65350

r	39	41	43	45	47	
$\mathcal{R}\left(QV_{r,2}(M_2)\right)$	12.27107	12.83540	13.01497	13.45313	13.99851	

Figure 6.3: Values of $\mathcal{R}\left(QV_{r,2}(M_2)\right)$ for several values of r.

We use the function **quantumvirog3(r,s)** for $s = 2$ and increasing values of r, and we obtain the following table of values of $\mathcal{R}\left(QV_{r,2}(M_3)\right)$ shown in Figure 6.4 and in Figure 5.4.

r	3	5	7	9	11	13
$\mathcal{R}\left(QV_{r,2}(M_3)\right)$	4.35517	11.49177	12.80934	13.58615	14.12955	14.53997

r	15	17	19	21	23	25
$\mathcal{R}\left(QV_{r,2}(M_3)\right)$	14.86388	15.12724	15.34618	15.53141	15.69039	15.82849

r	27	29	31			
$\mathcal{R}\left(QV_{r,2}(M_3)\right)$	15.94969	16.05691	16.12064			

Figure 6.4: Values of $\mathcal{R}\left(QV_{r,2}(M_3)\right)$ for several values of r.

Chapter 7

Conclusion

The goal of this thesis was to numerically test Conjecture 1.1 for an hyperbolic 3-manifold with a boundary which has both a toroidal component and a totally geodesic boundary component of genus $g \geq 2$. We produced Numerical tests 5.2, 5.3 and 5.4 for two hyperbolic manifolds of this kind : M_2 and M_3. While Numerical tests 5.2 and 5.4 seem to support Conjecture 1.1. Numerical test 5.3 does not. This raises questions that could be answered in further works.

To improve upon this thesis, we could compute $QV_{r,2}(M_2)$ and $QV_{r,2}(M_3)$ for bigger values of r. This could be done either by improving the code of Section 6.2 or by using greater computational resources such as the supercomputing facilities of the Université catholique de Louvain (CISM/UCL) and the Consortium des Équipements de Calcul Intensif en Fédération Wallonie Bruxelles (CÉCI). We should also have a careful examination of the code to make sure Numerical test 5.3 is correct. If the diverging behaviour is still seen as r grows larger and larger and as the code is meticulously verified, this could well be a counter-example to Conjecture 1.1.

In the early version [2] of [3], Chen-Yang proposed an extension of Conjecture 1.1.

Conjecture 7.1 (Conjecture 4.1, [2], Chen-Yang)**.** *Let M be a compact hyperbolic 3-manifold and $s \geq 1$. Then for r running over all integers such that $r \geq 3$ and $r \notin s\mathbb{N}$,*

$$\lim_{r\to\infty} \frac{s\pi}{r-2} \log\left(TV_{r,s}(M)\right) = Vol_H(M),$$

where $Vol_H(M)$ is the hyperbolic volume of M.

Functions constructed in Section 6.2 can already be used by the interested reader to test Conjecture 7.1.

Another way we could improve on this work is by testing Conjecture 1.1 for other compact hyperbolic 3-manifolds with an ideal triangulation, especially those with totally geodesic boundary of genus $g \geq 2$.

Bibliography

[1] Fathi Ben Aribi, François Guéritaud, and Eiichi Piguet-Nakazawa. Geometric triangulations and the teichmüller tqft volume conjecture for twist knots. 2020. arXiv 1903.09480.

[2] Qingtao Chen and Tian Yang. A volume conjecture for a family of turaev-viro type invariants of 3-manifolds with boundary. 2015. arXiv 1503.02547v2.

[3] Qingtao Chen and Tian Yang. Volume conjectures for the Reshetikhin-Turaev and the Turaev-Viro invariants. *Quantum Topol.*, 9(3):419–460, 2018.

[4] Renaud Detcherry, Efstratia Kalfagianni, and Tian Yang. Turaev-Viro invariants, colored Jones polynomials, and volume. *Quantum Topol.*, 9(4):775–813, 2018.

[5] R. Frigerio. An infinite family of hyperbolic graph complements in S^3. *J. Knot Theory Ramifications*, 14(4):479–496, 2005.

[6] Damian Heard. Orb: Reference, 2007. https://github.com/DamianHeard/orb/blob/master/OrbDocumentation.pdf.

[7] Vaughan F. R. Jones. A polynomial invariant for knots via von Neumann algebras. *Bull. Amer. Math. Soc. (N.S.)*, 12(1):103–111, 1985.

[8] R. M. Kashaev. The hyperbolic volume of knots from the quantum dilogarithm. *Lett. Math. Phys.*, 39(3):269–275, 1997.

[9] Rinat Kashaev, Feng Luo, and Grigory Vartanov. A TQFT of Turaev-Viro type on shaped triangulations. *Ann. Henri Poincaré*, 17(5):1109–1143, 2016.

[10] G. D. Mostow. Quasi-conformal mappings in n-space and the rigidity of hyperbolic space forms. *Inst. Hautes Études Sci. Publ. Math.*, (34):53–104, 1968.

[11] Tomotada Ohtsuki. On the asymptotic expansion of the quantum SU(2) invariant at $q = \exp(4\pi\sqrt{-1}/N)$ for closed hyperbolic 3-manifolds obtained by integral surgery along the figure-eight knot. *Algebr. Geom. Topol.*, 18(7):4187–4274, 2018.

[12] Jessica S. Purcell. *Hyperbolic knot theory*, volume 209 of *Graduate Studies in Mathematics*. American Mathematical Society, Providence, RI, [2020] ©2020.

[13] Akira Ushijima. A volume formula for generalised hyperbolic tetrahedra. In *Non-Euclidean geometries*, volume 581 of *Math. Appl. (N. Y.)*, pages 249–265. Springer, New York, 2006.

[14] Ka Ho Wong. Asymptotics of some quantum invariants of the whitehead chains. 2020. arXiv 1912.10638.